Rev.Adv.Mater.Sci. 19(2009) 41-62

A HOMOGENIZATION SCHEME FOR THE PLASTIC PROPERTIES OF NANOCRYSTALLINE MATERIALS

George J. Weng

Department of Mechanical and Aerospace Engineering, Rutgers University, New Brunswick, NJ 08903, USA

Received: November 22, 2008

Abstract. In this review we highlight a micromechanics-based homogenization scheme that has wide applicability for calculations of the overall rate-independent plasticity, time-dependent creep, strain-rate sensitivity, effect of porosity, and void growth for nanocrystalline materials. Based on the morphology disclosed in molecular dynamic simulation, we establish a composite model to represent the grain interior and the grain-boundary zone (GB zone). The nonlinear rate-independent plasticity is formulated in terms of the secant moduli of the constituent phases, whereas the rate-dependent viscoplasticity is formulated in terms of their secant viscosity. In both cases the heterogeneous stress and strain fields of the constituent phases are analytically determined. Through two related field fluctuation approaches, the effective stresses of the grain interior and the GB zone are derived through the variation of the overall secant moduli and the overall secant viscosity with respect to the constituent property. The overall behavior then can be calculated from the effective secant moduli or effective secant viscosity. We demonstrate how this approach provides the overall stress-strain relation as the grain size decreases from the coarse grain to the nanometer range, and how the slope of the Hall-Petch plot continues to decrease and eventually turns into negative below certain critical grain size. This critical grain size also gives rice to the maximum yield strength, and is an important factor in material design. We also show how the creep resistance increases with decreasing grain size and then decline, how the strain-rate sensitivity of the nanocrystalline materials is affected by grain size, and how porosity and grain size compete with each other under a constant strain rate loading. We conclude by the study of void growth during viscoplastic deformation of nanocrystalline materials.

1. INTRODUCTION

Plastic properties of nanocrystalline materials exhibit certain similarity to their coarse-grained counterparts, but due to the fine grain size significant departure is also present. Most notable among the various differences is the widely observed departure from the Hall-Petch relation in their yield strength [1,2]. This relation, $\sigma_y = \sigma_0 + k \cdot d^{-1/2}$ (where σ_0 is the Peierl stress, k the Hall-Petch slope, and d the grain size), is known to hold for a wide range of grain size, and it can be interpreted by the dislocation pile-up model [3] as well as by the dislocation density model [4]. But since the yield strength would tend to infinity as $d \rightarrow 0$, it cannot be expected to hold for very fine grain size. After nanocrystalline materials could be processed [5], many experiments have been conducted to examine the precise nature of grain size dependence over the nano-meter range. Some have reported a departure from this linear relation [6-8], while others have reported a negative slope in the Hall-Petch plot [9-11]. Such grain-size softening was initially attributed to the presence of sample imperfections such as voids or micro-cracks, but higher quality samples later prepared still showed a similar trend [12-14]. It is now generally believed that the departure from the Hall-Petch relation and the negative slope are not artifacts but rather genuine properties of nanocrystalline materials.

Corresponding author: George J. Weng, e-mail: weng@jove.rutgers.edu

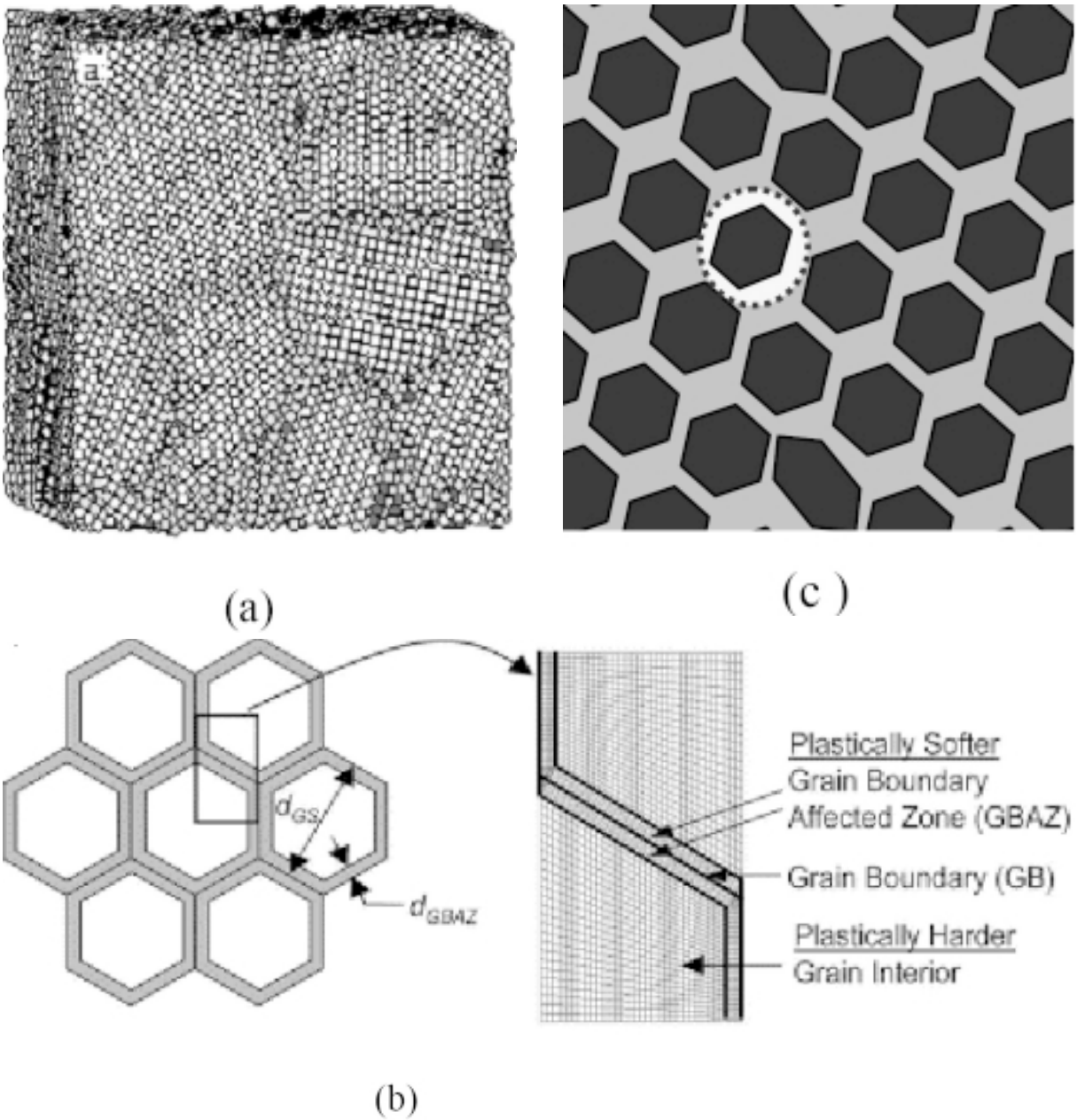

Fig. 1. (a) Morphology of a nanocrystalline metal by molecular dynamic simulation (Schiotz *et al.* 1998), (b) the plastically harder grain interior and the plastically softer GBAZ (Schwaiger *et al.* 2003), and (c) the 2-phase composite model with the grain interior and GBAZ.

At present the complicated deformation and failure mechanisms in nanocrystalline materials are still sunder intensive investigation, and the fields are still evolving. But many theories have been proposed to interpret the observed hardening and softening behavior. Nieh and Wadsworth [15] have studied the equilibrium position of dislocation pile-ups and arrived at a critical grain size below which the grains could not sustain the pile-up configuration. This was interpreted as the Hall-Petch break down, and the value was calculated to be about 19.3 nm for copper and 11.2 nm for palladium. Also based on the pile-up model, Wang *et al.* [16] have used the theoretical shear strength and the Peierl

strength to obtain the upper and lower bounds, respectively, of the critical grain size. Then through the geometrical means they found the critical size of 8.2 nm for copper and 11.6 nm for palladium. To provide a better understanding on the underlying deformation process, Gutkin *et al.* [17-20], and Gutkin and Ovid'ko [21] have suggested a cross-over mechanism from grain-boundary sliding to grain-boundary rotation, and they have also considered triple junctions as obstacles to GB sliding and grain-boundary migration as a rotational deformation mode. Most nanocrystalline materials processed so far have higher yield strength than their coarse-grained counterparts, but this is often offset by the undesirable reduction of ductility. In order to improve this important mechanical property significant efforts have also been made through various processing routes (Jia *et al.* [22]; Wang *et al*. 2002 [23,24]; Ma [25]; Zhao *et al.* [26]). It is beyond the scope to recall all the works here. Interested readers may refer to Jia *et al.* [27], Wei *et al.* [28,29], Han *et al*. [30], Ovid'ko [31], Ovid'ko and Sheinerman [32], Joshi and Ramesh [33,34], and Mayer *et al.* [35], among others.

On a different front, many molecular dynamic (MD) simulations have been conducted to uncover the properties of nanocrystalline materials [36-43]. These MD simulations have revealed a morphology with a high percentage of atoms in the grain-boundary region (see Fig. 1a), and the calculated results under constant strain-rate loading have confirmed that, as the grain size reached some critical value (usually below 10 nm), grain-size softening indeed could occur. Additional MD simulations on various face-centered and body-centered materials have further identified other operating mechanisms, but they all tend to support the general trend of grain-size hardening and softening as the size decreased [44-47].

Since atoms inside the grain boundary can move relative to each other in an uncorrelated fashion [36], the movement can generate significant amount of plastic strain and, when coupled with its increasing volume concentration with decreasing grain size, this contribution can be quite significant. This becomes all the more important, for the grain boundary is the continuous phase and is plastically softer than the grain interior. As such, its plastic activity can have a vital effect in lowering the yield strength of nanocrystalline materials. MD simulation is a powerful tool in disclosing the morphology and providing physical insights, but its calculations are limited to very small grain size and to very high strain rate. For instance in Schiotz *et. al.* [36] the largest grain size used was 13.2 nm, and the lowest strain rate was $2.5 \cdot 10^7$/s. With d = 6.56 nm, it already took 1,000,000 atoms to simulate the polycrystal behavior. At present, this approach cannot be realistically used to uncover the properties of nanocrystalline materials over a wide range of grain size and strain rate that are commonly encountered in experiments. These constraints point to the need of continuum modeling as an alternate route.

This is the concept of composite modeling. In this approach, and in line with the morphology disclosed by MD simulations, grains and grain-boundary are considered as two separate phases, each having its own properties. Early models however only employed very simple mixture rule. For instance Carsley *et al.* [48] adopted the Hall-Petch type hardness for the bulk phase and a glassy, amorphous phase with a constant strength for the grain-boundary phase, and used the rule of mixture to calculate the hardness of nickel, iron, and copper. Despite its simplicity this approach did provide a positive slope and then a negative one in the Hall-Petch plot. In a more sophisticated study Wang *et al.* [16] considered the simultaneous existence of an intracrystalline grain phase and an intercrystalline phase that is composed of the grain boundary, triple line, and quadruple node, and adopted different properties for each of them. Their calculations also showed significant deviation from the linear Hall-Petch relation ad small grain size. This multi-phase morphology was also adopted by Kim *et al.* [49] to calculate the strain-rate sensitivity of nanocrystalline solids. The crystallites were taken to obey a unified viscoplastic constitutive law, whereas the other regions were represented by the Naborro-Herring creep and Coble creep, with the grain-size dependence scaled with d^{-2} and d^{-3}, respectively. In this way they also demonstrated the significant grain-size hardening and softening. Other calculations based on the composite model can be attributed to Meyers and his associates [50-52], who made us of an earlier concept with an inner core to represent the grain interior and an outer shell to represent the work-hardening layer near the grain boundary [53]. Their calculations gave the expected Hall-Petch relation in the coarse grain region, then departure from it, and eventually reaching a constant, asymptotic value for the yield strength.

While these early composite models did provide important explanations for the observed grain-size hardening and softening, they all adopted the simple mixture law. That is, despite the different mechanical properties assigned to the grains and

the grain boundary region, these models took the stresses in all constituent phases to be the same, and were set equal to the externally applied ones. This is apparently a lower-bound calculation in the sense of Reuss. A more accurate approach is to adopt a micromechanics principle by which the stress heterogeneity can be adequately accounted for. Recognizing such a need, Jiang and Weng [54] first developed a dual-phase homogenization scheme to study the rate-independent plastic behavior of nanocrystalline metals. This approach was later extended to study the compressive yield strength of nanocrystalline ceramics [55], and extended to examine the grain-size dependence of yield strength of nanocrystalline polycrystals [56]. The issue of strain-rate sensitivity was taken up in Li and Weng [57], and the problem of high-temperature creep was most recently studied in Barai and Weng [58]. Due to the frequent presence of porosity associated with ball milling and compaction process, they further developed a 3-phase theory to examine the simultaneous contributions of grain size and porosity toward the overall viscoplastic properties of nanocrystalline materials [59]. In these studies the distinct morphology with grains serving as isolated inclusions and the GB zone as the continuous matrix phase was incorporated.

A related approach which also recognized the need to differentiate the heterogeneous state of stress and strain between the grains and grain boundary was developed by Capolungo *et al.* [60-63]. This study adopted the self-consistent scheme for the calculation of overall viscoplastic property. The self-consistent formulation however puts the grains and grain boundary on equal geometrical footing, and thus interchanging their geometrical arrangement would not produce different results for the overall composite. This is a major difference between this approach and the ones developed in [54-59]. We believe it is more preferable to consider the morphological separation between the grains and GB zone in the development of micromechanics theories for nanocrystalline materials, and this is what we plan to do in this review.

2. MOPHOLOGY OF THE COMPOSITE MODEL

Based on the morphology of a nanocrystalline material revealed from atomic simulations (Fig. 1a), it is evident that significant portion of atoms resides in the grain boundary region. A scanning transmission microscopy study on an electrodeposited nanocrystalline nickel indicated that a grain-boundary affected zone could appear and it could span over 7-10 lattice parameters into the grain. This region was depicted as the grain-boundary affected zone (GBAZ) in Fig. 1b [64], and was plastically softer than the grain interior. A general schematic representation of the 2-phase composite is shown in Fig. 1c, with the grain interior existing as inclusions and the GB zone as the matrix. They will be referred to as phase 1 and phase 0, with the respective volume concentrations, c_1 and c_0. It follows that,

$$c_1 = \left(\frac{d-t}{t}\right)^3 \quad \text{and} \quad c_0 = 1 - c_1, \tag{1}$$

where d is the grain size and t the thickness of the GB zone. Based on the lattice constant of Ni at 0.325 nm, the thickness t of the GBAZ is about 2.5-3.5 nm. If we use t = 3 nm as an average, the volume concentration of the GB zone,c_0, is about 27% with d = 30 nm, and as grain size decreases to 15 nm, its volume concentration can reach 49%. Since the GB zone is plastically softer than the grain interior, its increasing presence will cause the behavior of a nanocrystalline solid to depart from its coarse-grained counterpart. This is the source of departure from the Hall-Petch equation and the eventual decline of the yield strength.

3. A COMPOSITE MODEL FOR THE EFFECTIVE ELASTIC PROPERTIES OF NANOCRYSTALLINE MATERIALS

For the effective moduli of a nanocrystalline material the morphological distinction between the grain interior and the GB zone can be treated by either the Mori-Tanaka approach as developed in Weng [65-67], or by Christensen and Lo's [68] generalized self-consistent scheme. For the rate-independent problems in [54-56] we have adopted the generalized scheme as the starting point, whereas for the more involved rate-dependent problems in [57-59] we have used the Mori-Tanaka moduli as the starting point. In the elastic context neither approach will ever violate the Hashin-Shtrikman [69] and Walpole [70] bounds.

Upon an external loading the instantaneous response of a nanocrystalline material is elastic. My means of the Mori-Tanaka approach the overall elastic moduli can be calculated from [65]

$$\kappa = \kappa_0\left[1+\frac{c_1(\kappa_1-\kappa_0)}{c_0\alpha_0(\kappa_1-\kappa_0)+\kappa_0}\right],\ \mu = \mu\left[1+\frac{c_1(\mu_1-\mu_0)}{c_0\beta_0(\mu_1-\mu_0)+\mu_0}\right], \tag{2}$$

where, in terms of the Poisson's ratio, v_0, of the matrix

$$\alpha_0 = \frac{(1+v_0)}{3(1-v_0)},\ \beta_0 = \frac{2(4-5v_0)}{15(1-v_0)}. \tag{3}$$

These results are known to coincide with the Hashin-Shtrikman [69] lower (or upper) bounds if the matrix is the softer (or harder) phase, and even if one phase is harder (or softer) in bulk modulus and softer (or harder) in shear modulus, the calculated results will not violate Walpole's bounds [70]. The generalized self-consistent scheme also gives the same bulk modulus, but the shear modulus μ satisfies the quadratic equation

$$A\mu^2 + B\mu + C = 0, \tag{4}$$

where coefficients *A*, *B*, and *C* depend on the constituent moduli and their volume fractions and are listed in their original work with a later correction [68].

In a 3-phase composite, with the additional phase, called phase 2, still serving as inclusions inside the matrix, the effective bulk and shear moduli can be cast into [65]

$$\begin{aligned}
\frac{\kappa}{\kappa_0} &= 1+\frac{(c_1+c_2)\alpha_0(\kappa_1-\kappa_0)(\kappa_2-\kappa_0)+c_1\kappa_0(\kappa_1-\kappa_0)+c_2\kappa_0(\kappa_2-\kappa_0)}{\kappa_0^2+(1-c_2)\alpha_0\kappa_0(\kappa_2-\kappa_0)+(1-c_1)\alpha_0\kappa_0(\kappa_1-\kappa_0)+\left[1-(c_1+c_2)\right]\alpha_0^2(\kappa_1-\kappa_0)(\kappa_2-\kappa_0)} \\
\frac{\mu}{\mu_0} &= 1+\frac{(c_1+c_2)\beta_0(\mu_1-\mu_0)(\mu_2-\mu_0)+c_1\mu_0(\mu_1-\mu_0)+c_2\mu_0(\mu_2-\mu_0)}{\mu_0^2+(1-c_2)\beta_0\mu_0(\mu_2-\mu_0)+(1-c_1)\beta_0\mu_0(\mu_1-\mu_0)+\left[1-(c_1+c_2)\right]\alpha_0^2(\mu_1-\mu_0)(\mu_2-\mu_0)}
\end{aligned} \tag{5}$$

in parallel to (2). This set is useful for the study of multiphase nanocrystalline solid, or to evaluate the influence of porosity.

In elastic response the average hydrostatic and deviatoric components of stress of the constituent phases are related to the externally applied stress of the composite, $\overline{\sigma}_{ij}$, as

$$\begin{aligned}
\sigma_{kk}^{(1)} &= \frac{\kappa_1}{(c_1+c_0\alpha_0)(\kappa_1-\kappa_0)+\kappa_0}\overline{\sigma}_{kk},\ \sigma_{kk}^{'(1)} = \frac{\mu_1}{(c_1+c_0\beta_0)(\mu_1-\mu_0)+\mu_0}\overline{\sigma}_{kk}; \\
\sigma_{kk}^{(1)} &= \frac{\alpha_0(\kappa_1-\kappa_0)+\kappa_0}{(c_1+c_0\alpha_0)(\kappa_1-\kappa_0)+\kappa_0}\overline{\sigma}_{kk},\ \sigma_{kk}^{'(1)} = \frac{\beta_0(\mu_1-\mu_0)+\mu_0}{(c_1+c_0\beta_0)(\mu_1-\mu_0)+\mu_0}\overline{\sigma}_{kk}.
\end{aligned} \tag{6}$$

where an overbear signifies that it is a volume-average quantity. In a three-phase system that gives rise to Eq. (5), these connections can be cast in the general form for the *r*-th phase as

$$\sigma_{kk}^{(r)} = \frac{\kappa_r}{\left[\alpha_0(\kappa_r-\kappa_0)+\kappa_0\right]\left[1+(1-\alpha_0)a\right]}\overline{\sigma}_{kk},\ \sigma_{ij}^{'(r)} = \frac{\mu_r}{\left[\beta_0(\mu_r-\mu_0)+\mu_0\right]\left[1+(1-\mu_0)b\right]}\overline{\sigma}_{ij}, \tag{7}$$

where

$$\begin{aligned}
a &= \sum_r \frac{c_r(\kappa_r-\kappa_0)}{\alpha_0(\kappa_r-\kappa_0)+\kappa_0}, \\
b &= \sum_r \frac{c_r(\mu_r-\mu_0)}{\beta_0(\mu_r-\mu_0)+\mu_0}.
\end{aligned} \tag{8}$$

These elastic stress states serve as the initial condition for the calculation of subsequent plastic deformation. The corresponding elastic strain components can be extracted from these stress components, and can be further extended to calculate the strain history of a viscoelastic composite through the Laplace transform, and other time- and rate-dependent processes for the nonlinear composites.

4. NONLINEAR CONSTITUTIVE EQUATIONS OF THE GRAIN INTEIOR AND GB ZONE

After the initial elastic response, the nonlinear plastic or viscoplastic deformation follows. Before we proceed to present the homogenization schemes we first outline the nonlinear constitutive equations for both the grain interior and the grain-boundary zone. The properties of the grain interior represented the orientational means of the anisotropic constituent crystallites according to its crystal structure (Weng [71]; Jiang and Weng [56]), and are isotropic.

4.1. Rate-independent plasticity

The nonlinear stress-strain relation of the isotropic, grain interior phase can be written as

$$\sigma_e = \sigma_y^{(g)} + h_g \cdot \left(\varepsilon_e^p\right)^{n_g}, \tag{9}$$

where σ_e is the effective stress and ε_e^p is the effective plastic strain, defined by

$$\sigma_e = \left(\frac{3}{2}\sigma'_{ij}\sigma'_{ij}\right)^{1/2}, \quad \varepsilon_e^p = \left(\frac{2}{3}\varepsilon_{ij}^p\varepsilon_{ij}^p\right)^{1/2}, \tag{10}$$

in terms of the deviatoric stress σ'_{ij}, and plastic strain ε_{ij}^p. Constants $\sigma_y^{(g)}$, h_g, and n_g are the yield stress, strength coefficient, and work-hardening exponent, of the grain interior, in turn.

For the grain interior, both $\sigma_y^{(g)}$ and h_g are grain-size dependent, and can be written to follow the Hall-Petch relation, as

$$\sigma_y^{(g)} = \sigma_{y(g)}^{\infty} + k \cdot d^{-\frac{1}{2}}, \quad h_g = h_g^{\infty} + a \cdot d^{-\frac{1}{2}}, \tag{11}$$

where $\sigma_{y(g)}^{\infty}$, k, h_g^{∞} and a are material constants for the grain interior. The behavior of the GB zone is not grain-size dependent, but due to its largely amorphous nature as revealed in Fig. 1a, it will be taken to be pressure-dependent. To this end we invoke Drucker's pressure-dependent yield criterion for the GB zone, as [72]

$$\sigma_e = \sigma_y^{(gb)} + m \cdot p + h_{gb} \cdot \left(\varepsilon_e^p\right)^{n_{gb}}, \tag{12}$$

where $\sigma_y^{(gb)}$, m, and h_{gb} are its properties, and the pressure, $p = -\sigma_{kk}/3$. The presence of m is the main source for the tension-compression asymmetry of a nanocrystalline material.

At a given state of deformation, the secant Young's modulus of the grain interior, denoted by E_g^s, the secant Poisson's ratio v_g^s, and the secant bulk and shear moduli, can be evaluated from

$$E_g^s = \frac{1}{\dfrac{1}{E_g} + \dfrac{\varepsilon_{e(g)}^p}{\sigma_e^{(g)}}}, \quad v_g^s = \frac{1}{2} - \left(\frac{1}{2} - v_g\right)\frac{E_g^s}{E_g}.$$
$$\kappa_g^s = \frac{E_g^s}{3\left(1-2v_g^s\right)}, \quad \mu_g^s = \frac{E_g^s}{2\left(1+v_g^s\right)}. \tag{13}$$

Those of the GB phase can be written in a similar fashion.

4.2. Rate-dependent constitutive relations

For calculations of time-dependent creep, strain-rate sensitivity, and void growth in nanocrystalline solids, the rate-dependent constitutive equations of the grain interior and GB zone need to be specified. These in general can be described by the unified constitutive equation, as

$$\dot{\varepsilon}_e^{vp} = \dot{\varepsilon}_e^{vp} \cdot \left(\frac{\sigma_e}{s}\right)^n, \tag{14}$$

where $\dot{\varepsilon}_e^{vp}$ is the effective viscoplastic strain rate, defined as in (10) but cast in the rate form, n is the stress exponent, and s the drag stress. The reference strain rate $\dot{\varepsilon}_e^{vp}$ is a scaling factor that can be set arbitrarily. Due to work hardening the drag stress increases with deformation; it can be taken to be controlled by the competition between strain hardening and dynamic recovery as

$$\dot{s} = h \cdot \left(1 - \frac{s}{s_*}\right)\dot{\varepsilon}_e^{vp}, \quad \text{or} \quad s = s_* - \left(s_* - s_0\right)e^{\frac{\varepsilon_e^{vp}}{s_*/h}} \tag{15}$$

upon integration, with s_0 representing the initial hardening state and s_* the final saturation state. There are three material constants involved in the rate equations: n, s_0, and s_*.

This set of constitutive relations applies to both the grain interior and GB zone. Since the drag stress represents the hardening state of the phase, it can be taken to follow the Hall-Petch equation for the grain interior again, now as

$$s_0^{(g)} = s_0^{\infty} + kd^{-1/2}, \quad s_*^{(g)} = as_0^{(g)}. \tag{16}$$

This k of course is not to be confused with the k in (11) for the rate-independent theory. The behavior of the GB zone is again taken to be grain-size independent, so only $s_0^{(gb)}$ and $s_*^{(gb)}$ are involved.

For such an elastic-viscoplastic phase, say phase r, its secant viscosity η_r^s is defined through

$$\dot{\varepsilon}_{ij}^{vp(r)} = \frac{1}{2\eta_r^s}\sigma_{ij}^{'(r)}, \quad \text{or} \quad \dot{\varepsilon}_{ij}^{vp(r)} = \frac{1}{3\eta_r^s}\sigma_e^{(r)}. \tag{17}$$

After making use of the Prandtl-Reuss relation the secant viscosity can be written specifically for the grain interior (phase 1) and GB zone (phase 0), as

$$\eta_1^s = \frac{s^{(g)}}{3\dot{\varepsilon}_e^{vp}} \cdot \left(\frac{\dot{\varepsilon}_e^{vp}}{\dot{\varepsilon}_0^{vp}}\right)^{1/n^{(g)}}, \quad \eta_0^s = \frac{s^{(gb)}}{3\dot{\varepsilon}_e^{vp}} \cdot \left(\frac{\dot{\varepsilon}_e^{vp}}{\dot{\varepsilon}_0^{vp}}\right)^{1/n^{(gb)}}. \tag{18}$$

In the linear comparison composite, the secant moduli in (13) and the secant viscosity in (18) will continue to replace the elastic moduli and the Maxwell viscosity, respectively, of the constituent phases in applying the results of a linear elastic and a linear viscoelastic composite to the rate-independent and the rate-dependent deformation of nanocrystalline materials.

5. A HOMOGENIZATION SCHEME FOR THE RATE-INDEPENDENT PLASTICITY OF NANOCRYSTALLINE MATERIALS

The basis of the nonlinear homogenization scheme to be presented here is a linear comparison composite that carries an identical microgeometry as the nonlinear problem. In the rate-independent case the elastic moduli of the constituent phases are successively replaced by their secant moduli. Replacement of the nonlinear relation by a linear one through the secant moduli can be traced back to Berveiller and Zaoui [73] in the self-consistent formulation of polycrystal plasticity, in which the tangent moduli of the constituent grains in Hill's [74] incremental scheme were replaced by the secant moduli. The secant moduli formulation was adopted by Weng [75] in his calculation of polycrystal plasticity, and the results were found to compare well with Hutchinson's [76] results based on Hill's incremental relation. Formal presentation of a comparison composite can be dated back to Talbot and Willis [77]. Since then it has been developed into various forms (*e.g.* Tandon and Weng [78]; Weng [79]; Ponte Castaneda [80]; Willis [81]; Qiu and Weng [82]; Suquet [83]; Hu [84]). There are also other nonlinear approaches for the heterogeneous solids (e.g. Accorsi and Nemat-Nasser [85]; Dvorak [86]; Mason *et al.* [87]; Doghri and Tinel [88]; Berbenni et al. [89]; Nemat-Nasser and Hori [90]). For the rate-independent behavior one may choose either Eq. (2) or Eq. (4) as the starting point for the elastic response. Eq. (2) has the merit of being more explicit but Eq. (4) applies better to the higher concentration. For the rate-independent plasticity we take the generalized self-consistent formulation, with the secant moduli as

$$\kappa_s = \kappa_{gb}^s\left[1 + \frac{c_g\left(\kappa_g^s - \kappa_{gb}^s\right)}{c_{gb}\alpha_{gb}^s\left(\kappa_g^s - \kappa_{gb}^s\right) + \kappa_{gb}^s}\right],$$
$$A\mu_s^2 + B\mu_s + C = 0, \tag{19}$$

where the subscript or superscript s stands for the secant moduli, g for the grain interior, and gb for the grain-boundary zone.

A key step now is to find the secant moduli of the grain interior and GB zone at a given level of applied stress, $\bar{\sigma}_{ij}$. In view of (13) and (9), the secant moduli in turn depend on the effective stress $\sigma_{e(r)}$ of the constituent phase r. This quantity can be most conveniently evaluated by the field fluctuation approach as conceived in Bobeth and Diener [91], and Kreher and Pompe [92] in a linear elastic solid, and applied by Hu [84] to the rate-independent plasticity. For a pressure-dependent constituent phase, this procedure further leads to [54]

$$\sigma_{e(r)}^2 = \frac{1}{c_r}\left[\frac{1}{3}\left(\frac{\mu_r^s}{\kappa_c^s}\right)^2\frac{\partial\kappa_c^s}{\partial\mu_r^s}\bar{\sigma}_{kk}^2 + \left(\frac{\mu_r^s}{\mu_c^s}\right)^2\frac{\partial\mu_c^s}{\partial\mu_r^s}\bar{\sigma}_e^2\right],$$
$$\sigma_{kk(r)}^2 = \frac{1}{c_r}\left[\left(\frac{\kappa_r^s}{\kappa_c^s}\right)^2\frac{\partial\kappa_c^s}{\partial\kappa_r^s}\bar{\sigma}_{kk}^2 + 3\left(\frac{\kappa_r^s}{\kappa_c^s}\right)^2\frac{\partial\mu_c^s}{\partial\kappa_r^s}\bar{\sigma}_e^2\right]. \tag{20}$$

The pressure in the grain-boundary phase is given by $p = -(1/3)\sigma_{kk}^{(gb)}$.

The nonlinear stress-strain relation of the nanocrystalline solid now can be calculated by gradually increasing the applied stress, $\bar{\sigma}_{ij}$. The initial response is elastic. For a given grain size d, the volume concentrations, c_1 and c_0 of the grain

interior and GB zone are calculated from Eq. (1), and the elastic moduli of the nanocrystalline material are determined from (2) and (4), and this gives the linear elastic response. Upon plastic yielding, the effective stress of the constituent phase is determined from (20), and used in the constitutive equations to calculate its secant moduli, which are in turn used in (19) to calculate the effective secant moduli of the nanocrystalline material. Then the overall strain at a given level of stress follows from

$$\bar{\varepsilon}_{kk} = \bar{\sigma}_{kk} / (3\kappa_s), \quad \bar{\varepsilon}'_{ij} = \bar{\sigma}'_{ij} / (2\mu_s). \tag{21}$$

The entire stress-strain curve of the nanocrystalline material at a given grain size can be obtained by increasing the level of applied stress to obtain the new level of overall strain through the obtained effective secant bulk and shear moduli, κ_s and μ_s.

6. A HOMOGENIZATION SCHEME FOR THE RATE-DEPENDENT VISCOPLASTIC RESPONSE

In order to develop a nonlinear, rate-dependent homogenization model that remains explicit, we will adopt a unified scheme that translates the effective elastic response into a linear viscoelastic one through the Laplace transform, and then replace the Maxwell viscosity of the constituent phase by the secant viscosity given in (18). The correspondence principle for a viscoelastic composite was first introduced by Hashin [93], and applied by Wang and Weng [94] and Li and Weng [95] to study the influence of inclusion shape on the creep, strain-rate sensitivity, and relaxation behavior of a two-phase composite material. The concept of secant viscosity, on the other hand, was initially introduced by Li and Weng [96-98] to study the creep and viscoplastic behavior of a metal-matrix composite. As the Laplace transform and its inversion back to the real space involve some cumbersome operation, it is easier to adopt Eq. (2) for the effective elastic moduli. While Eq. (3) can also be used as the starting point, the resulting expression is quite lengthy and proves to be rather inconvenient for implementation in the field fluctuation approach.

Before we proceed to give results based on the Laplace transform-inversion process, we first recall a simple effective secant viscosity approach that can be readily used for the determination of strain-rate sensitivity of a fully compact nanocrystalline material.

6.1. A simple secant viscosity approach for the strain-rate sensitivity of perfectly compact nanocrystalline materials

In the absence of porosity and when both constituent phases are plastically incompressible, overall plastic dilatation is not a critical factor. In this case we may assume the overall response to be also plastically incompressible, with the effective shear viscosity [57]

$$\eta_c = \eta_0 \left[1 + \frac{c_1(\eta_1 - \eta_0)}{\frac{2}{5} c_0(\eta_1 - \eta_0) + \eta_0} \right],$$
$$\text{or} \quad \eta_c = \eta_0 \left[1 + \frac{c_1(1-R)}{\frac{2}{5} c_0(1-R) + R} \right], \tag{22}$$

by way of the effective shear modulus in (2), where $R = \eta_0 / \eta_1$, is the ratio of viscosity of the matrix and inclusions. (This equation reduces to Einstein's $\eta = \eta_0(1 + 2.5c_1)$ for rigid dilute suspensions in a Newtonian fluid). The overall deviatoric stress of the nanocrystalline solid, $\bar{\sigma}'_{ij}$, and its overall viscoplastic strain-rate, $\dot{\bar{\varepsilon}}^{vp}_{ij}$ then follows from

$$\bar{\sigma}'_{ij} = 2\eta^s_c \dot{\bar{\varepsilon}}^{vp}_{ij}, \tag{23}$$

where the effective secant viscosity of the composite, η^s_c, has identical form as η_c in (22) but with the linear Maxwell viscosities η_1 and η_0 replaced by their secant counterparts in (18).

Based on consideration of overall work rate of the composite, the field-fluctuation approach can be applied to establish the connections between the strain-rate of the constituent phase and that of the overall composite by local variation of effective viscosity of the individual phase. Details can be found in [57], and the results are

$$\dot{\bar{\varepsilon}}^{vp(1)}_e = \left(\frac{1}{c_1} \frac{\partial \eta^s}{\partial \eta^s_1} \right)^{1/2} \dot{\bar{\varepsilon}}^{vp}_e, \quad \dot{\bar{\varepsilon}}^{vp(0)}_e = \left(\frac{1}{c_0} \frac{\partial \eta^s}{\partial \eta^s_0} \right)^{1/2} \dot{\bar{\varepsilon}}^{vp}_e, \tag{24}$$

where, from (22), we have

$$\frac{\partial \eta^s}{\partial \eta^s_1} = \frac{c_1 R^2}{\left[\frac{2}{5} c_0(1-R) + R \right]^2},$$
$$\frac{\partial \eta^s}{\partial \eta^s_0} = \left[1 + \frac{c_1}{\frac{2}{5} c_0(1-R) + R} \right] \cdot \left[1 + \frac{c_1}{\frac{2}{5} c_0(1-R) + R} \right]. \tag{25}$$

Back to (18), these relations provide the secant viscosity of the grain interior and the GB zone, and then back to (22) (with viscosity replaced by the secant viscosity) for the effective secant viscosity of the composite at a given stage of deformation. With the help of (23) the overall stress-rate of the composite can be evaluated from $\dot{\bar{\sigma}}_{ij} = C_{ijlk}\left(\dot{\bar{\varepsilon}}_{ij} - \dot{\bar{\varepsilon}}^{vp}_{ij}\right)$, where C_{ijlk} is the overall elastic moduli of the dual-phase system, given by (2). The overall stress-strain relation of the nanocrystalline solid then can be determined in an incremental manner.

6.2. A unified scheme from elasticity to viscoelasticity to viscoplasticity

A more widely usable scheme that is not restricted with the assumption of overall plastic incompressibility is to carry out the Laplace transform and inversion completely. We take the dilatational response of both grain interior and GB zone to be purely elastic. In this case the effective bulk and shear moduli of the effective medium in the transformed domain – to be denoted by the superscripts "TD" – can be written as

$$\kappa^{TD} = \kappa_0\left[1+\frac{c_1(\kappa_1-\kappa_0)}{c_0\alpha_0^{TD}(\kappa_1-\kappa_0)+\kappa_0}\right],$$
$$\mu^{TD} = \mu_0^{TD}\left[1+\frac{c_1(\mu_1^{TD}-\mu_0^{TD})}{c_0\beta_0^{TD}(\mu_1^{TD}-\mu_0^{TD})+\mu_0^{TD}}\right], \qquad (26)$$

in parallel to (2), where μ_r^{TD} is the shear modulus of *r*-th phase in the Laplace space, related to the transformed stress, denoted by a hut "^", through

$$\hat{\bar{\sigma}}_{kk}^{(r)} = 3\kappa_r^{TD}\hat{\bar{\varepsilon}}_{kk}^{(r)},\ \hat{\bar{\sigma}}'^{(r)}_{kk} = 2\mu_r^{TD}\hat{\bar{\varepsilon}}_{ij}^{(r)},\ r=0,1, \qquad (27)$$

and α_r^{TD} and β_r^{TD} follow from Eq. (3), as

$$\alpha_0^{TD} = \frac{3\kappa_0}{3\kappa_0+4\mu_0^{TD}},\ \beta_0^{TD} = \frac{6}{5}\frac{\kappa_0+2\mu_0^{TD}}{3\kappa_0+4\mu_0^{TD}}. \qquad (28)$$

Due to the decomposition of total strain rate into the elastic and viscoplastic components in our problem, the simplest linear model is the Maxwell element, with a shear viscosity η_r for the *r-th* phase. In this case the transformed shear modulus can be written as

$$\mu_r^{TD} = \frac{\mu_r s}{s+T_r},\ \text{with}\ T_r = \frac{\mu_r}{\eta_r},\ r=0,1 \qquad (29)$$

The effective stress and strain of the dual-phase material in the Laplace space are then related to each other through

$$\hat{\bar{\sigma}}_{kk} = 3\kappa^{TD}\hat{\bar{\varepsilon}}_{kk},\ \hat{\bar{\sigma}}'_{ij} = 2\mu^{TD}\hat{\bar{\varepsilon}}'_{ij}. \qquad (30)$$

Upon Laplace inversion, this set of equations will give the time- or rate-dependent response of the dual-phase material under a prescribed loading. We now consider two important loading conditions: i) the time-dependent creep under a constant stress, and ii) the stress-strain relation under a constant strain-rate.

6.2.1. Time-dependent creep of a nanocrystalline material under a constant stress

This procedure can be used to calculate the development of creep strain of a linear viscoelastic composite under a constant stress $\bar{\sigma}_{ij}$ = const. In this case $\hat{\bar{\sigma}}_{ij} = \bar{\sigma}_{ij}/s$, where *s* is the Laplace parameter, and Laplace inversion for the strain results in

$$\bar{\varepsilon}_{kk}(t) = \frac{1}{3\kappa_0}\cdot\frac{y_3}{y_1}\left[1+A+\frac{B}{y_1}\exp\left(-\frac{y_2}{y_1}t\right)\right]\bar{\sigma}_{kk},$$
$$\bar{\varepsilon}'_{ij}(t) = \frac{1}{2\mu_0}\Big[C+D\cdot t+ p\exp(-rt)\left(\cos(wt)+\frac{q-r}{w}\sin(wt)\right)\Big]\bar{\sigma}'_{ij}, \qquad (31)$$

for the development of creep strain. Constants *A*, *B*, …*etc.* depend on the viscosities η_1 and η_0, and volume concentration c_1; they could be found in [58].

Due to the continuous change of secant viscosity of the constituent phases in the viscoplastic case, this total form should not be used directly. Instead, its incremental form should be adopted, as

$$\dot{\bar{\varepsilon}}_{kk} = \frac{1}{3\kappa_0}\cdot\frac{y_3 b_1}{y_1^2}\cdot\exp\left(-\frac{y_2}{y_1}t\right)\bar{\sigma}_{kk},$$
$$\dot{\bar{\varepsilon}}'_{ij} = \frac{1}{2\mu_0}\Big[D+p(-r)\exp(-rt)\big(\cos(wt)+ \frac{q-r}{w}\sin(wt)\big)+p\exp(-rt)\{-w\sin(wt)+ (q-r)\cos(wt)\}\Big]\bar{\sigma}'_{ij}. \qquad (32)$$

This rate equation allows one to introduce the concept of effective secant viscosities, η_κ^s and η_μ^s, through

$$\bar{\sigma}_{kk}(t) = 3\eta_{\kappa}^{s}(t)\dot{\bar{\varepsilon}}_{kk},\ \ \bar{\sigma}'_{ij}(t) = 2\eta_{\mu}^{s}(t)\dot{\bar{\varepsilon}}'_{ij}, \tag{33}$$

where

$$\begin{aligned}
&\frac{1}{\eta_{\kappa}^{s}(t)} = \frac{1}{\kappa_0}\cdot\frac{y_3 b_1}{y_1^2}\left[\exp\left(-\frac{y_2}{y_1}t\right)\right],\\
&\frac{1}{\eta_{\kappa}^{s}(t)} = \frac{1}{\mu_0}\Big[D + p(-r)\exp(-rt)\big(\cos(wt) +\\
&\frac{q-r}{w}\sin(wt)\big) + p\exp(-rt)\{-w\sin(wt) +\\
&(q-r)\cos(wt)\}\Big].
\end{aligned} \tag{34}$$

As in the rate-independent case, extension of this linear viscoelastic composite to the nonlinear viscoplastic composite will require determination of the secant viscosity of the constituent phases, η_1^s and η_0^s in (18), and this in turn requires determination of the effective stress, $\sigma_e^{(r)}$. This again, can be determined from the field fluctuation approach by considering the work-rate equivalence. The result is [58]

$$\begin{aligned}
&\sigma_e^{(r)2} = \frac{\mu_r}{c_r}\left[\frac{\partial}{\partial T_r}\left(\frac{1}{\eta_{\mu}^{s}}\right)\cdot\bar{\sigma}_e^2 +\right.\\
&\left.\frac{\partial}{\partial T_r}\left(\frac{1}{\eta_{\kappa}^{s}}\right)\cdot\frac{\bar{\sigma}_{kk}^2}{3}\right],\ \ r = 0,1
\end{aligned} \tag{35}$$

Once $\sigma_e^{(r)}$ is known for an individual phase, its secant viscosity can be calculated from the constitutive equation (18). The overall strain rate follows from (32), and the development of creep strain can be calculated incrementally by

$$\bar{\varepsilon}_{ij}(t+\Delta t) = \bar{\varepsilon}_{ij}(t) + \dot{\bar{\varepsilon}}_{ij}(t)\cdot\Delta t, \tag{36}$$

with the increment of time, Δt.

6.2.2. Strain-rate sensitivity under the combined effect of grain size and porosity

Under a constant strain-rate loading $\dot{\bar{\varepsilon}}_{ij}$ = const., one has $\hat{\dot{\bar{\varepsilon}}}_{ij} = (1/s^2)\cdot\dot{\bar{\varepsilon}}_{ij}$. Laplace inversion then leads to

$$\bar{\sigma}_{kk}(t) = 3\eta_{\kappa}(t)\dot{\bar{\varepsilon}}_{kk},\ \ \bar{\sigma}'_{ij}(t) = 2\eta_{\mu}\dot{\bar{\varepsilon}}'_{ij}, \tag{37}$$

where for a nanocrystalline material that contains some porosity, the effective elastic moduli of the material is given by (5), with phase 2 representing the voids (i.e. κ_2=μ_2=0). Direct application of Eq. (5) to the viscoelastic state under a constant strain rate leads to

$$\begin{aligned}
&\eta_{\kappa}(t) = \kappa_0\Big\{A + pe^{-n}\Big[\cos(wt) +\\
&\frac{q-r}{w}\sin(wt)\Big]\Big\},\\
&\eta_{\mu}(t) = \left(1+\frac{x_4}{x_8}\right)\eta_0 - (\eta_0-\delta)e^{-T_0 t} +\\
&E\Big\{F_1 e^{\lambda_1 t} + e^{a_1 t}\Big[(F_2+F_3)\cos(b_1 t) +\\
&(F_2-F_3)\sin(b_1 t)\Big]\Big\},
\end{aligned} \tag{38}$$

where constants *A, p, q, … etc.* also depend on the constituent viscosities and volume concentrations; they could be found in [59]. This equation reduces to the perfectly compact case with c_2=0.

Due to the continuous change of secant viscosity of the constituent phases, Eqs. (37) and (38) must again be used in the incremental form. That is,

$$\dot{\bar{\sigma}}_{kk}(t) = 3\dot{\eta}_{\kappa}^{s}(t)\dot{\bar{\varepsilon}}_{kk},\ \ \dot{\bar{\sigma}}'_{ij}(t) = 2\dot{\eta}_{\mu}^{s}(t)\dot{\bar{\varepsilon}}'_{ij}, \tag{39}$$

where the effective dilatational and shear secant-viscosity rates are given by

$$\begin{aligned}
&\dot{\eta}_{\kappa}^{s} = \kappa_0\Big\{-pre^{-rt}\Big[\cos(wt) +\\
&\frac{q-r}{w}\sin(wt)\Big] + pe^{-rt}\Big[-w\sin(wt) +\\
&(q-r)\cos(wt)\Big]\Big\},\\
&\dot{\eta}_{\mu}^{s} = T_0(\eta_0-\delta)e^{-T_0 t} + E\Big\{F_1\lambda_1 e^{\lambda_1 t} +\\
&+a_1 e^{a_1 t}\Big[(F_2+F_3)\cos(b_1 t)+(F_2-F_3)\sin(b_1 t)\Big] +\\
&e^{a_1 t}\Big[-(F_2+F_3)b_1\sin(b_1 t)+(F_2-F_3)b_1\cos(b_1 t)\Big]\Big\}.
\end{aligned} \tag{40}$$

respectively. The nonlinear viscoplastic response of the nanocrystalline solid then can be determined through this linear viscoelastic comparison composite by replacing the Maxwell viscosities η_0 and η_1 by their respective secant viscosities.

The corresponding results derived from the field-fluctuation principle under a constant strain-rate loading give rise to the connection between the effective viscoplastic strain rates of the constituent phase $\dot{\bar{\varepsilon}}_e^{vp(r)}$ with the applied strain rate $\dot{\bar{\varepsilon}}_{ij}$ as

Table 1. Material constants used in calculations for the rate-independent plasticity of copper.

Material Property	Grain Interior	GB Zone
E(GPa)	108.0	92.0
ν	0.33	0.33
σy(MPa)	259.0	145.0
h(GPa)	0.688	0.48
n	0.5	0.4
k(GPa$\sqrt{nm}$)	1.38	——
a(GPa$\sqrt{nm}$)	0.243	——
m	——	0.4

$$\dot{\bar{\varepsilon}}_e^{vp(1)} = \left[\frac{1}{c_1}\left(\frac{1}{3}\frac{\partial\eta_\kappa^s}{\partial\eta_1^s}\left(\dot{\bar{\varepsilon}}_{kk}\right)^2 + \frac{\partial\eta_\mu^s}{\partial\eta_1^s}\dot{\bar{\varepsilon}}_e^2\right)\right]^{1/2},$$
$$\dot{\bar{\varepsilon}}_e^{vp(0)} = \left[\frac{1}{c_0}\left(\frac{1}{3}\frac{\partial\eta_\kappa^s}{\partial\eta_0^s}\left(\dot{\bar{\varepsilon}}_{kk}\right)^2 + \frac{\partial\eta_\mu^s}{\partial\eta_0^s}\dot{\bar{\varepsilon}}_e^2\right)\right]^{1/2}, \quad (41)$$

These effective strain rates can be used in the constitutive Eq. (18) to calculate the secant viscosity of the individual phase. The stress rate then follows from (39) and (40), and the entire stress-strain curve of the nanocrystalline solid for a given grain size and porosity can be calculated incrementally, as

$$\bar{\sigma}_{kk}(t+\Delta t) = \bar{\sigma}_{kk}(t) + \dot{\bar{\sigma}}_{kk}\Delta t,$$
$$\bar{\sigma}'_{ij}(t+\Delta t) = \bar{\sigma}'_{ij}(t) + \dot{\bar{\sigma}}'_{ij}\Delta t. \quad (42)$$

6.2.3. Evolution of porosity and void growth in the nanocrystalline solids

In addition, evolution of porosity and the process of void growth during the constant strain-rate loading can be determined from

$$c_2 = \frac{V_2}{V}, \text{ or } \dot{c}_2 = \frac{\dot{V}_2}{V} - \frac{V_2\dot{V}}{V^2} = c_2\left(\dot{\bar{\varepsilon}}_{kk}^{(2)} - \dot{\bar{\varepsilon}}_{kk}\right), \quad (43)$$

where V_2 and V are the volume of the voids and the composite, respectively. The dilatational rate of the voids, $\dot{\bar{\varepsilon}}_{kk}^{(2)}$, is given by

$$\dot{\bar{\varepsilon}}_{kk}^{(2)} = \left\{B - pre^{-rt}\left[\cos wt + \frac{q-r}{w}\sin wt\right] + pe^{-rt}\left[-w\sin wt + (q-r)\cos wt\right]\right\}\dot{\bar{\varepsilon}}_{kk}. \quad (44)$$

7. STUDY OF RATE-INDEPENDNT PLASTICITY, TIME-DEPPENDENT CREEP, STRAIN-RATE SENSITIVITY, AND EFFECT OF POROSITY ON SEVERAL NANOCRYSTALLINE MATERIALS

The preceding homogenization scheme can be used to study several fundamental properties of nanocrystalline materials. We now show some of the calculated results.

7.1. Grain-size effect on the rate-independent stress-strain relation of nanocrystalline copper

The homogenization scheme outlined in Sect. 5, in conjunction with the rate-independent constitutive equations of the grain interior and GB zone given in Sect. 3.1, has been applied to study the grain-size effect of nanocrystalline copper. Such a material has been tested by Sanders *et al*. [12,13]. The material properties used in the model are listed in Table 1. Following the suggestion of Chokshi *et al*. [9] and Kim *et al*. [49], we took the GB thickness to be t = 1 nm in the calculations. The experimental stress-strain curves of the copper with its grain size decreasing from 20 μm to 26 nm are shown in Fig. 2a, whereas the calculated results are shown in Fig. 2b. Both indicate a strong grain-size dependence of the stress-strain behavior. As grain size decreases from the coarse 20 μm to the nano 26 nm, there is a continuous strengthening of the plastic response. However, the increase from 20 mm to 110 nm is seen to be far more significant than the increase from 49 nm to 26 nm. This is a strong indication of the decline in the slope of Hall-Petch plot over this range of grain size. The Hall-Petch plot at 0.2% yield strength is shown in Fig. 3 for both experiment and theory, where a departure from the linear relation is vividly shown. The experiment was conducted under tension, under which the theoretical curve further provides a critical grain size of about 44 nm after which the slope becomes negative. This is the critical state at which the material has its highest yield strength. The tension-compression asymmetry of the nanocrystalline

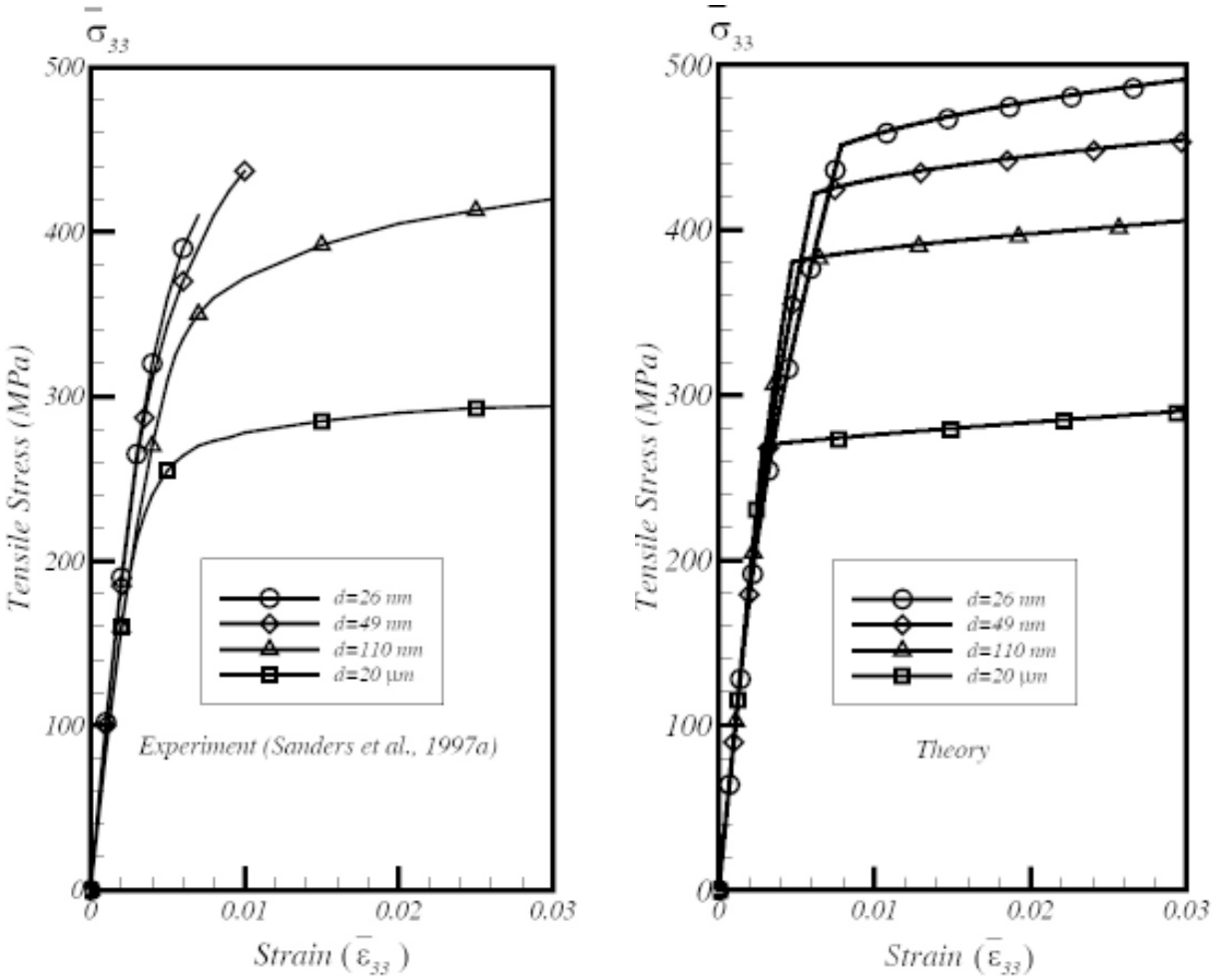

Fig. 2. Tensile stress-strain relations of copper as a function of grain size *d*: (a) experimental data of Sanders *et al.*(1997a), and (b) theoretical predictions.

copper as calculated from the model is also illustrated here. This asymmetry arises from the pressure-dependence of the constitutive relation of the GB zone as represented by the parameter, *m*, in Eq. (12). The ratio of the computed yield stress to the tensile yield stress is about 2.4, which is close to their test value of 2.3. The critical grain size at which the slope turns into negative also becomes smaller under compression, at about 16 nm.

7.2. Grain-size effect on the time-dependent creep deformation of nanocrystalline copper

The time-dependent, high-temperature creep deformation of nanocrystalline materials can be calculated with the homogenization scheme outlined in Sect. 6.2.1, in conjunction with the rate-dependent constitutive equations of the grain interior and GB zone given in Sect. 4.2. In order to account for the temperature effect, the Arrhenius function was introduced into the latter as

$$\dot{\varepsilon}_e^{vp} = \dot{\varepsilon}_0^{vp} \cdot \left(\frac{\sigma_e}{s} \right)^n \cdot \exp(-q / RT), \tag{45}$$

where Q is the activation energy, R the universal gas constant, and T the temperature in Kelvin. The Young's modulus in general decreases with increasing temperature in a linear fashion, as

$$E(T) = E_{RT}\left[1 - \alpha_T (T - T_{RT})\right], \tag{46}$$

for each phase, where the subscripts "*RT*" stand for room temperature, and α_T is the reduction coefficient. Other parts of the constitutive equations remain unchanged. We have used this approach

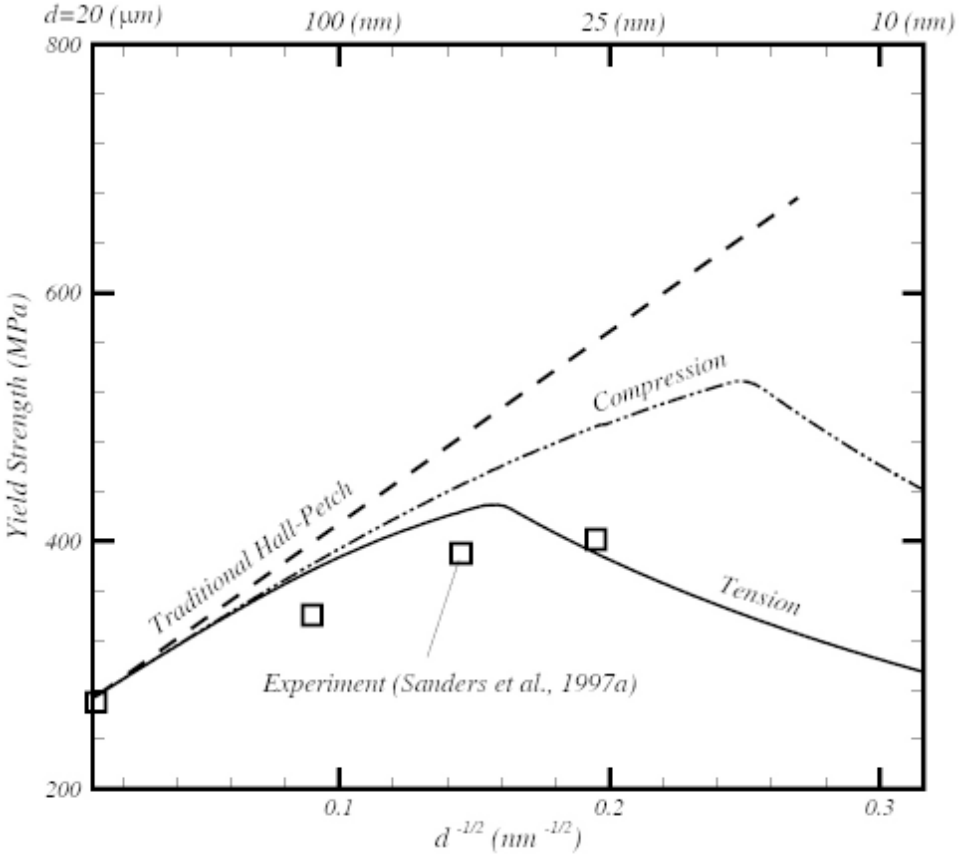

Fig. 3. Departure of the 0.2% yield stress from the Hall-Petch plot as the grain size decreases. The bottom four data points were taken from Fig. 3a under tension, and the top curve was calculated under compression. There is a significant strength-differential effect between tension and compression in the nano-meter range.

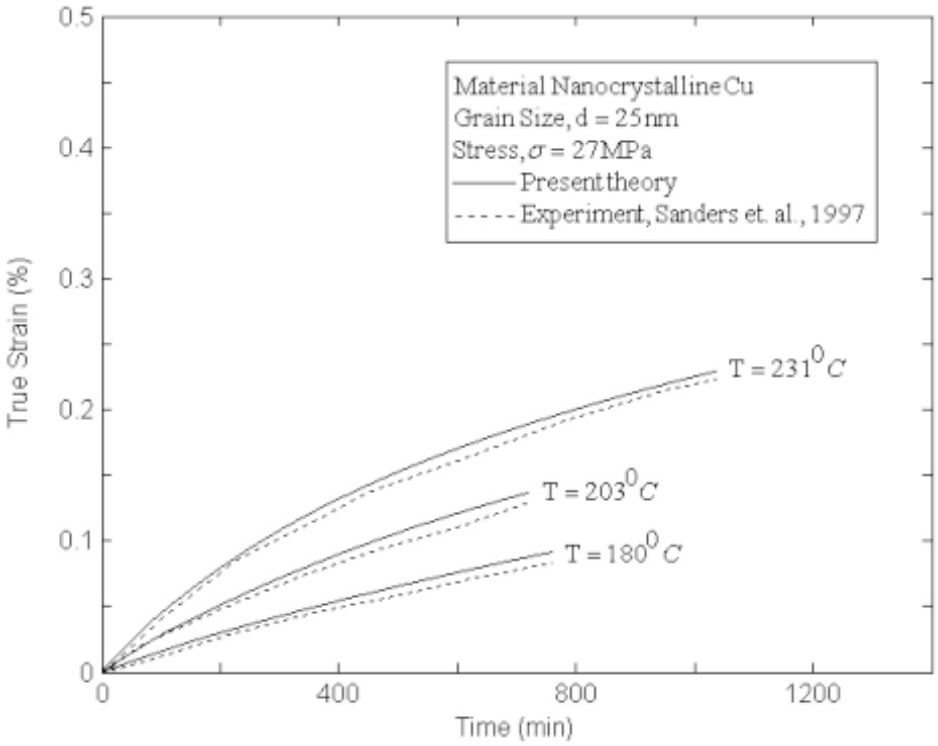

Fig. 4. Comparison between the developed theory and the test data of Sanders e*t. al. (*1997).

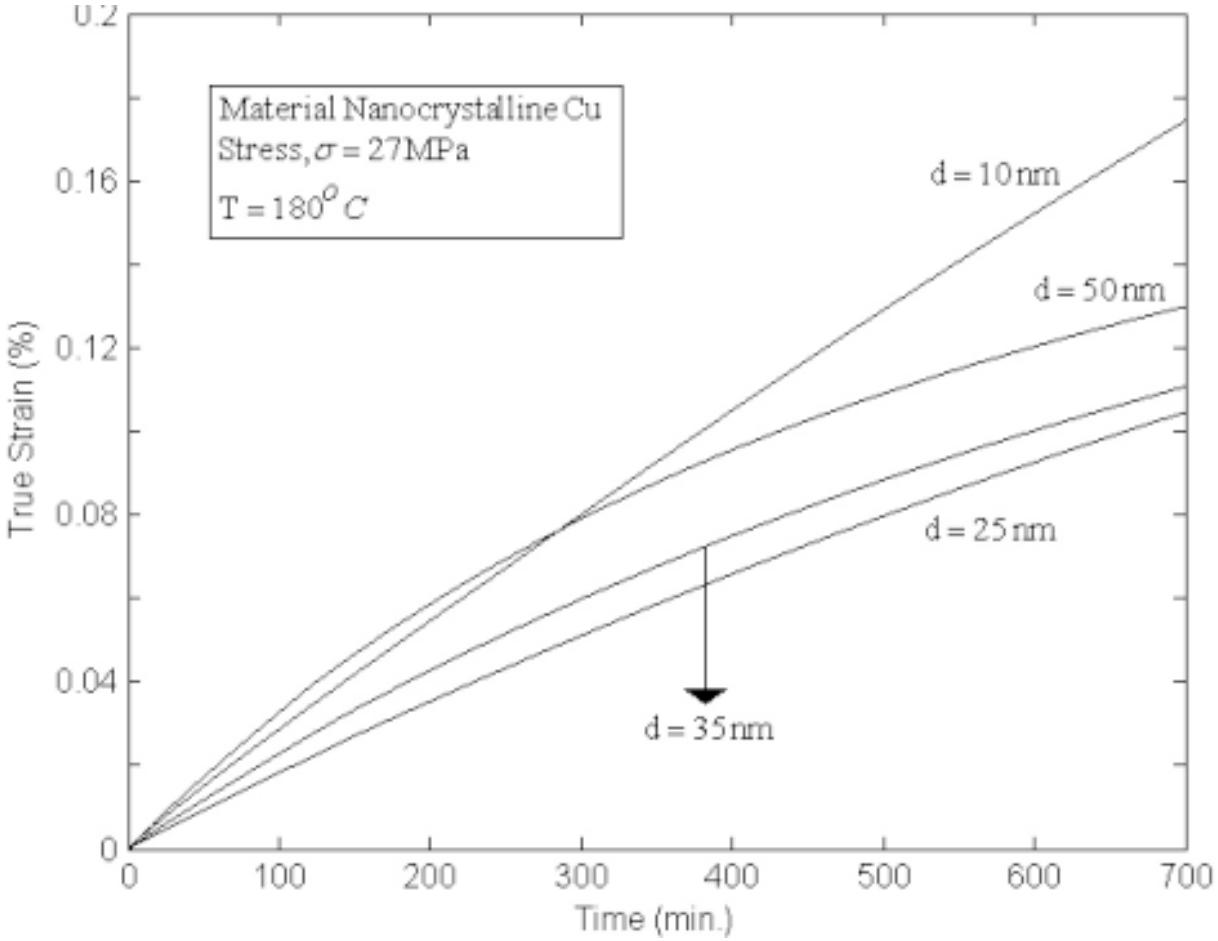

Fig. 5. Grain size hardening and softening of a nanocrystalline copper.

to evaluate the creep deformation of nanocrystalline copper, nickel, and NiP alloy [58].

The temperature-dependence of creep deformation for a nanocrystalline copper at the grain size of d = 25 nm, is illustrated in Fig. 4. Adopting the concept of GBAZ suggested in Schwaiger et al. [64] the thickness t was taken to be 3 nm in the calculations for creep. This test was conducted by Sanders *et al.* [99]. The material constants used here are listed in Table 2. The calculated theoretical curves are also plotted in Fig. 4. At T=180 °C, the theoretical results for the growth of creep strain spanning over the grain sizes of 50 nm to 10 nm are given in Fig. 5. It indicates that, as the gain size decreases from 50 nm to 25 nm, there is a continuous creep strengthening due to the decrease of grain size that can be attributed to the Hall-Petch effect to the grain interior, but as the grain size further decreases down to 10 nm, the increased contribution from the softer GB zone has led to the increase of creep strain. This is the inverse Hall-Petch effect of the nanocrystalline solid in creep deformation.

7.3. Strain-rate sensitivity of nanocrystalline nickel

In the absence of porosity the effective secant viscosity scheme given in Sect. 6.1 provides a direct approach to the calculation of strain-rate sensitivity of a nanocrystalline material. We applied it in conjunction with the rate-dependent constitutive relations in Sect. 4.2 to calculate the strain-rate sensitivity of nanocrystalline nickel over a wide range of grain size and strain rate. The material constants used in the model calculation are listed in Table 3, and, based on the concept of GBAZ, the thickness t was taken to be 3 nm. The calculated results for the grain-size dependence of stress-strain relation under a constant strain rate

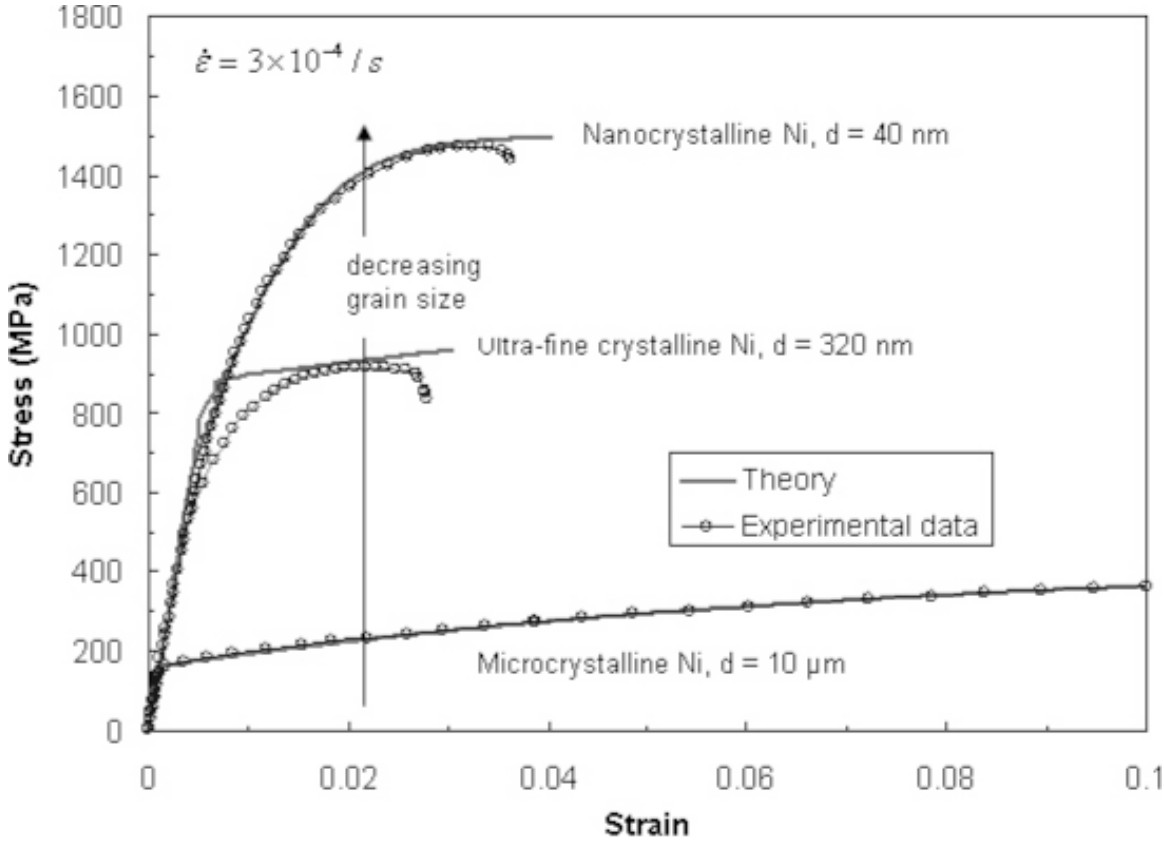

Fig. 6. Theoretical predictions and experimental data (Schwaiger *et al.* 2007) for the stress-strain relations of nickel with the grain sizes of 40 nm, 320 nm, and 10 μm.

Table 2. Material parameters used in calculations for creep of copper.

Material Property	Grain Interior	GB zone
E_{RT}(GPa)	120	120
α_T	0.0009	0.0007
ν	0.31	0.3
s_0(MPa)	—	130
s_*(MPa)	—	400
n	3.8	3.5
$s_0^{(\infty)}$(MPa)	5.5	—
k (MPa$\sqrt{nm}$)	1500	—
a	1.3	—
h (MPa)	20000	10000
Q (J/M)	17000	7000

Table 3. Material parameters used in calculations for strain-rate sensitivity of nickel.

Material Property	Grain Interior	GB Zone
E (GPa)	200	200
ν	0.3	0.3
$s_0^{(\infty)}$(MPa)	4.03	——
k (GPa$\sqrt{nm}$)	15.8	——
a	2.63	——
s_0 (MPa)	——	360
s_* (MPa)	——	820
h (MPa)	5.6	20
n	200	55
$\dot{\varepsilon}_0(10^{-4}/hr)$	1.0	1.0

loading of $\dot{\varepsilon} = 3\cdot10^{-4}$/s – from the microcrystalline size at $d = 10$ μm, to ultra-fine size at 320 nm, and further down to the nano size at 40 nm - are shown in Fig. 6, where the test data of Schwaiger *et al.* [64] are also displayed. The theory is seen to capture the measured data sufficiently well. To illustrate the strain-rate sensitivity of this nanocrystalline

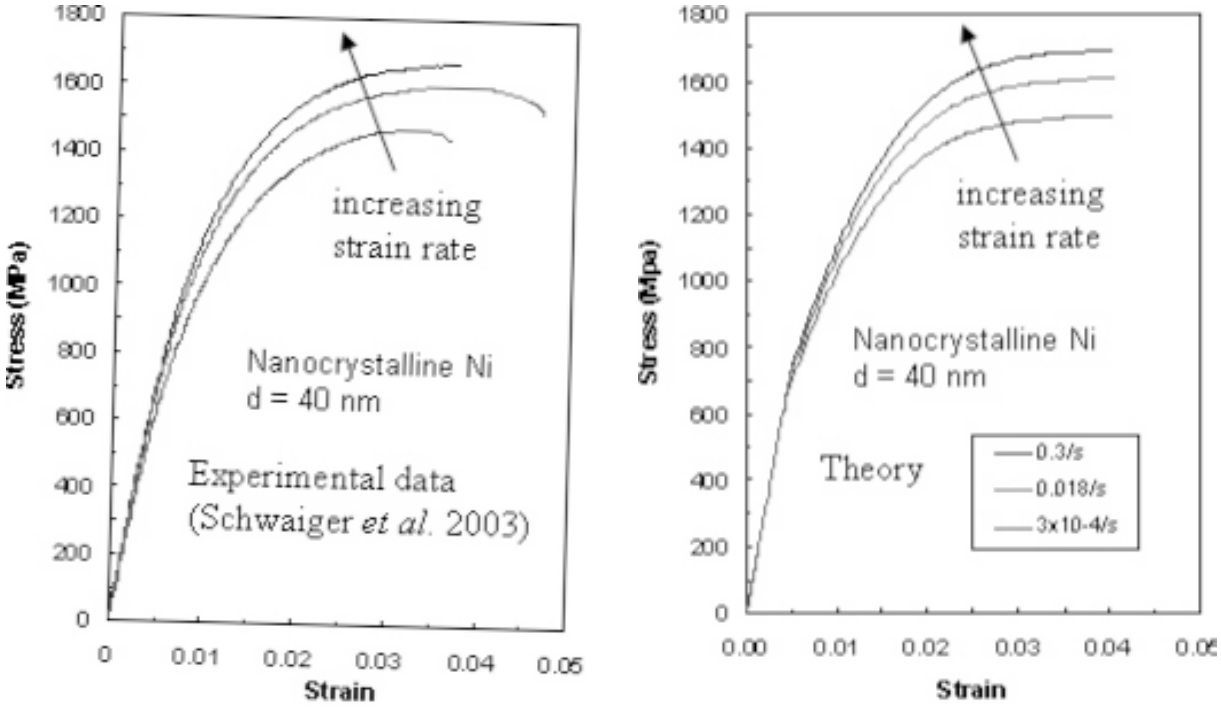

(a) (b)

Fig. 7. Strain-rate sensitivity of a nanocrystalline Ni with d = 40 nm: (a) experimental curves, and (b) theoretical calculations.

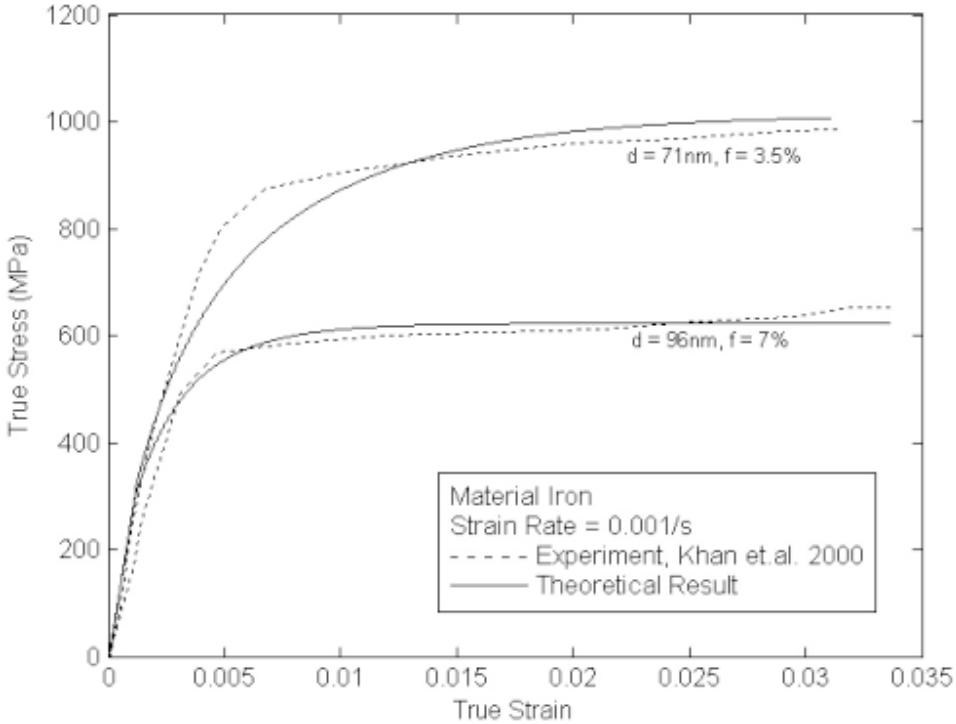

Fig. 8. Comparison between the experimental and theoretically obtained true stress strain relations under uniaxial compressive loading for nanocrystalline iron at a particular strain rate of 0.001/s with a grain size of 71 nm and 96 nm along with porosity (f) of f = 7% and 3.5%, respectively.

material, we also applied the theory to calculate the stress-strain relations at d = 40 nm. The test data and calculated results for $\dot{\varepsilon}$ = 0.3/s, 0.018/s, and $3 \cdot 10^{-4}$/s, are shown in Figs. 7a and 7b, respec-

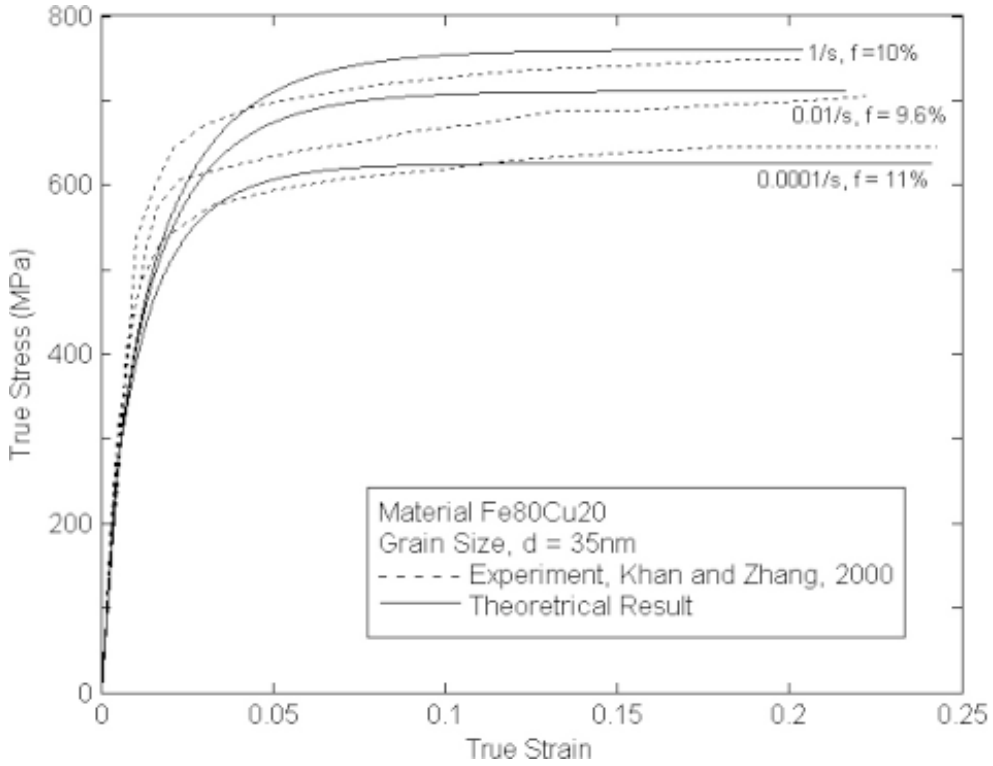

Fig. 9. Comparison between the experimental and theoretically obtained true stress strain relations under uniaxial compressive loading for nanocrystalline Fe80Cu20 with a grain size of 35nm and three different strain rate of 0.0001/s, 0.01/s and 1/s along with different porosity (*f)* of 11%, 9.6%, and 10% respectively.

tively, reflecting reasonable agreement between the two.

7.4. Effect of porosity on the strain-rate sensitivity of nanocrystalline iron and iron-copper mixture

With the presence of voids, a nanocrystalline material can become plastically compressible even if both grain interior and GB zone are both not. In this case the Laplace transform and inversion technique outlined in Sect. 6.2.2 will serve as a better approach for extension to the viscoplastic regime. We have used this approach to calculate the effect of porosity on the strain-rate sensitivity of nanocrystalline iron and iron-copper mixture tested by Khan *et al.* [100] and Khan and Zhang [101], respectively. The material constants used are listed in Table 4 for iron and Table 5 for Fe80Cu20 (wt.%). The results for the nanocrystalline iron at gain sizes d = 71 nm and 96 nm with the porosity of 3.5% and 7%, respectively, are shown in Fig. 8 under the rate of $\dot{\varepsilon}$ = 0.001/s. The calculated results are seen to be able to capture the simultaneous effect of grain size and porosity sufficiently well. The results for the nanocrystalline Fe80Cu20 under three different orders of strain rate at sufficiently high porosity are shown in Fig. 9. The measured data are again

Table 4. Material constants used in calculations for the effect of porosity on the strain-rate sensitivity of iron.

Material Property	Grain Interior	GB Zone
E (GPa)	210.0	210.0
ν	0.3	0.3
$s_0^{(\infty)}$ (MPa)	5.03	——
k (GPa$\sqrt{nm}$)	4.25	——
a	1.1	——
s_0 (MPa)	——	320
s_* (MPa)	——	600
h (MPa)	1	1.5
n	220	120
$\dot{\varepsilon}_0(10^{-4}/hr)$	1.0	1.0

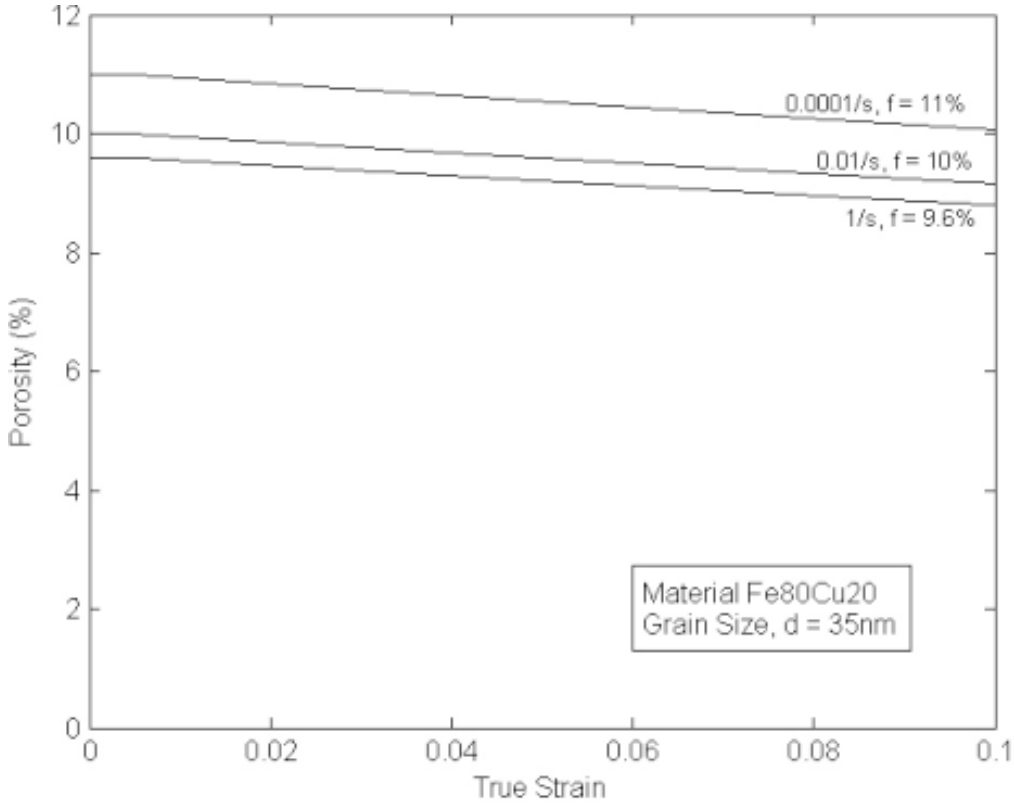

Fig 10. Change of porosity with strain in a nanocrystalline Fe80Cu20 alloy at d = 35 nm at ifferent initial porosities.

well modeled by the homogenization theory. Both Fe and Fe80Cu20 show relatively flat stress-strain behavior. This is believed to be due to the ball-milling technique used by Khan *et al.* As pointed out by Han *et al.* [30], this processing route tends to produce low work-hardening nanocrystalline materials.

7.5. Evolution of porosity under a constant strain-rate loading, and its influence on the reduction of Young's modulus under compression

Voids in a viscoplastic solid tend to grow under tension and shrink under compression. The principle given in Sect. 6.2.3 is capable of tracing the evolution of voids under a constant strain-rate loading. We have used the homogenization scheme in Sect. 6.2.2 in conjunction with this principle to calculate the evolution of voids in a nanocrystalline Fe80Cu20 (at the grain size of 35 nm) under compression with three initial void fractions. The results are shown in Fig. 10, under three distinct strain rates. These correspond to the loading conditions in Fig. 9, which were calculated with this set of porosity change as plastic deformation continued. At the end of 10% strain deformation, the normal-

Table 5. Material constants used in calculations for void growth under constant strain-rate loading of $Fe_{80}Cu_{20}$.

Material Property	Grain Interior	GB Zone
E (GPa)	70.0	70.0
ν	0.3	0.3
$s_0^{(\infty)}$ (MPa)	5.1	——
k (GPa$\sqrt{nm}$)	1.8	——
a	1.5	——
s_0 (MPa)	——	255
s_* (MPa)	——	600
h (MPa)	10	9
n	120	60
$\dot{\varepsilon}_0(10^{-4}/hr)$	1.0	1.0

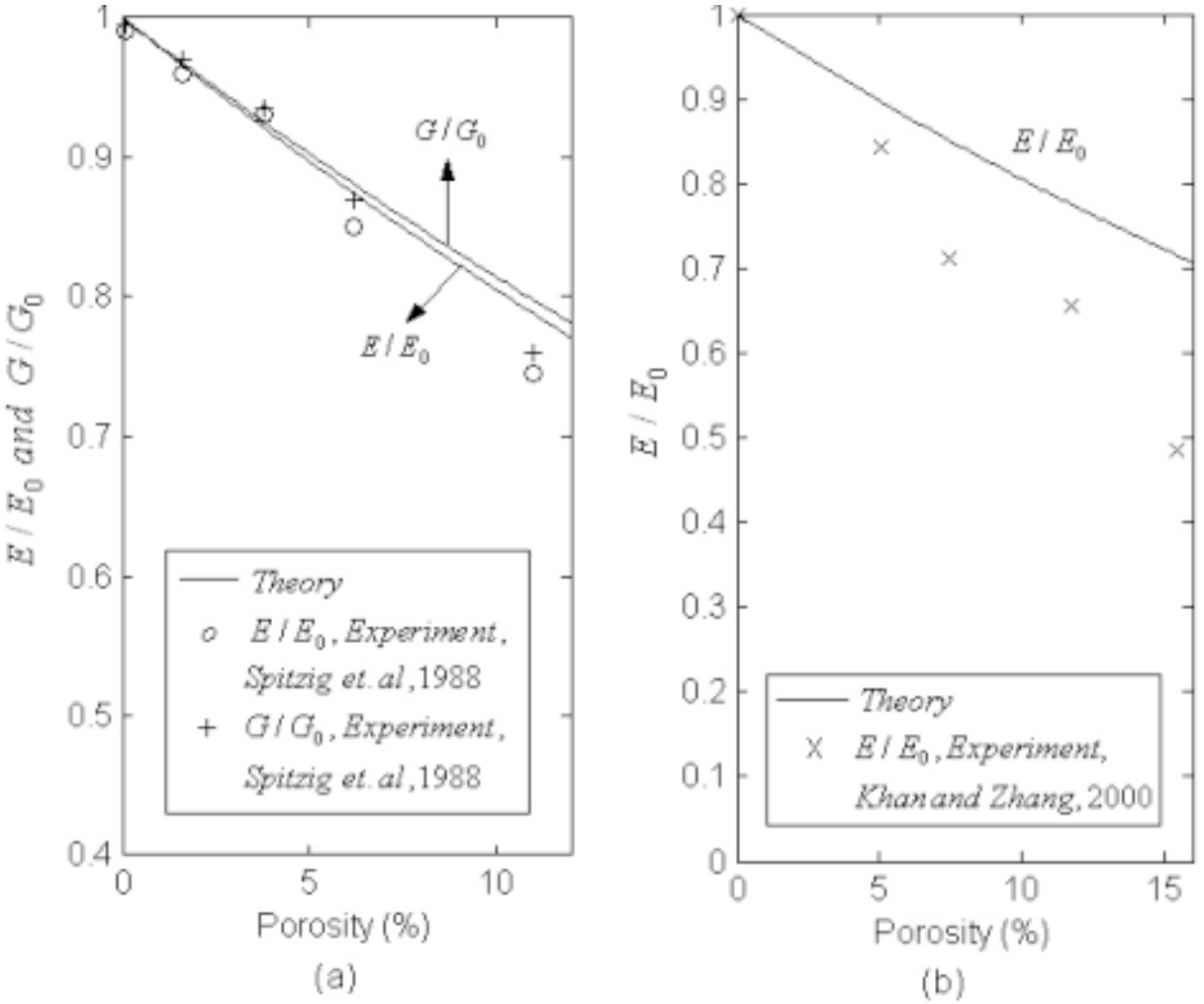

Fig. 11. Reduction in Young's modulus with increasing porosity. Comparison with the test data of Fe compacts (Spitzig *et al*. 1988) and nanocrystalline Fe80Cu20 (Khan and Zhang, 2000).

ized porosity has decreased to about 0.92 in all three cases. This compares well with the value of 0.91 in the compression test of Spitzig *et al.* [102] on iron compacts. Change of porosity naturally results in the change of Young's modulus for the material. We have also computed such dependence from Eq. (5) by setting phase 2 to be the voids. The calculated results are shown in Figs. 11a and 11b in sold lines. The test data of Spitzig *et al.* [102] for iron compacts and those of Khan and Zhang [101] for a nanocrystalline Fe80Cu20 (grain size d=23 nm) are also shown alongside. Comparison in the former is seen to be in good agreement, but the significant difference in the second case apparently requires further investigation.

8. CONCLUDING REMARKS

In this review we have highlighted a homogenization scheme that can be widely applied to calculate the rate-independent plastic response, the time-dependent creep deformation, the strain-rate sensitivity of a fully compacted nanocrystalline solid, the influence of porosity, and void growth, for this new class of materials. This scheme is based on a composite model in which the grain interior and the grain-boundary zone are represented by spherical inclusions and a continuous matrix, each having its own properties. We have treated the problems in the broad context of elasticity, rate-independent plasticity, and time- and rate-dependent viscoplasticity. The underlying homogenization

scheme is a linear comparison composite, which serves to extend the results of elasticity to the rate-independent plasticity through the secant moduli, and to extend the results of linear viscoelasticity to the nonlinear viscoplasticity through the secant viscosity. A key step in such extensions is the determination of effective stress or effective strain rate of the constituent phases at a given stage of deformation, and this was carried out with the application of field-fluctuation principles through energy balance for the rate-independent case, and through work-rate balance for the rate-dependent one. Once the overall secant moduli or the overall secant viscosity of the nanocrystalline solid is determined, its overall plastic or viscoplastic behavior can be calculated for a given grain size.

We have demonstrated that this approach can provide a myriad of properties for the nanocrystalline materials. These include the Hall-Petch effect and its departure as the grain size decreases from the coarse grain to the nano grain range, the tension-compression asymmetry, and the existence of a critical grain size at which the maximum yield strength occurs, and the maximum strength itself. This latter finding is of some technological significance in our pursuit for the optimal strength of a material. Such a critical grain size also exists for high-temperature creep resistance. We have also demonstrated how grain size and strain-rate can simultaneously affect the viscoplastic behavior of a nanocrystalline material, and how voids could lower the elastic moduli and plastic yield strength. This scheme can be further extended to examine other types of mechanical properties of nanocrystalline materials.

ACKNOWLEDGEMENT

This work was supported by the US National Science Foundation, Division of Civil, Mechanical and Manufacturing Innovation, Mechanics and Structure of Materials Program, under grant CMS-0510409.

REFERENCES

[1] E.O. Hall // *Proc. Phys. Soc.* **B64** (1951) 747.
[2] N.J. Petch // *J. Iron Steel Inst.* **174** (1953) 25.
[3] J.D. Eshelby, F.C. Frank and F.R.N. Naborro // *Phil. Mag*. **42** (1951) 351.
[4] H. Conrad, S. Feuerstein and L. Rice // *Mater. Sci. Engng.* **A2** (1967) 157.
[5] R. Birringer, H. Gleiter, H.-P. Klein and P. Marquardt // *Phys. Lett.* **102A** (1984) 365.
[6] G.W. Nieman, J.R. Weertman and R.W. Siegel // *J. Mater. Res*. **6** (1991) 1012.
[7] A.M. El-Sherik, U. Erb, G. Palumbo and K.T. Aust // *Scripta Metall.Mater,* **27** (1992) 1185.
[8] V.Y. Gertman, M. Hoffmann, H. Gleiter and R. Birringer // *Acta Metall.Mmater*. **42** (1994) 3539.
[9] A.H. Chokshi, A. Rosen, J. Karch and H. Gleiter // *Scripta Metall.* **23** (1989) 1679.
[10] L. Lu, M.L. Sui and K. Lu // *Science* **287** (2000) 1463.
[11] G.E. Fougere, J.R. Weertman, R.W. Siegel and S. Kim // *Scripta Metall. Mater*. **26** (1992) 1879.
[12] D.G. Sanders, C.J. Youngdahl and J.R. Weertman // *Mater. Sci. Engng*. **A234-236** (1997) 77.
[13] D.G. Sanders, J.A. Eastman and J.R. Weertman // *Acta Mater*. **45** (1997) 4019.
[14] J.R. Weertman, D. Farkas, K. Hemker, H. Kung, M. Mayo, R. Mitra and H. Van Swygenhoven // *MRS Bulletin* **24** (1999) 44.
[15] T.G. Nieh and J. Wadsworth // *Scripta Metall*. **25** (1991) 955.
[16] N. Wang, Z. Wang, K.T. Aust and U. Erb // *Acta Metall. Mater*. **43** (1995) 519.
[17] M.Y. Gutkin, I.A. Ovid'ko and N.V. Skiba // *Acta Mater*. **51** (2003) 4059.
[18] M.Y. Gutkin, I.A. Ovid'ko and N.V. Skiba // *J. Phys. D: Appl. Phys*. **36** (2003) L47.
[19] M.Y. Gutkin, I.A. Ovid'ko and C.S. Pande // *Phil. Mag*. **84** (2004) 847.
[20] M.Y. Gutkin, I.A. Ovid'ko and N.V. Skiba // *Acta Mater*. **52** (2004) 1711.
[21] M.Y. Gutkin and I.A. Ovid'ko // *Appl. Phys. Lett*. **87** (2005) 251916.
[22] D. Jia, Y.M. Wang, K.T. Ramesh, E. Ma, Y.T. Zhu and R.V. Valiev // *Appl. Phys. Lett*. **79** (2001) 611.
[23] Y.M. Wang, M.W. Chen, F.H. Zhou and E. Ma // *Nature* **419** (2002) 912.
[24] Y.M. Wang, E. Ma and M.W. Chen // *Appl. Phys. Lett*. **80** (2002) 2395.
[25] E. Ma // JOM April (2006) 49.
[26] Y.H. Zhao, J.F. Bingert, X.Z. Liao, B.Z. Cui, K. Han, A.V. Swergueeva, A.K. Mukherjee, R.Z. Valiev, T.G. Langdon and Y.T. Zhu // *Adv. Mater*. **18** (2006) 2949.
[27] D. Jia, K.T. Ramesh and E. Ma // *Acta Mater*. **51** (2003) 3495.
[28] Q. Wei, S. Cheng, K.T. Ramesh and E. Ma // *Mater. Sci. Engng*. **381** (2004) 71.

[29] Q. Wei, T. Jiao, K.T. Ramesh, E. Ma, L.J. Kecskes, L. Magness, R. Dowding, V.U. Kazykhanov and R.Z. Valiev // *Acta Mater*. **54** (2006) 77.
[30] B.Q. Han, E.J. Lavernia and F.A. Mohamed // *Rev. Adv. Mater. Sci*. **9** (2005) 1.
[31] I.A. Ovid'ko // *Rev. Adv. Mater. Sci*. **10** (2005) 89.
[32] I.A. Ovid'ko and A.G. Sheinerman // *Rev. Adv. Mater. Sci*. **16** (2007) 1.
[33] S.P. Joshi and K.T. Ramesh // *Scripta Mater*. **57** (2007) 877.
[34] S.P. Joshi and K.T. Ramesh // *Acta Mater*. **56** (2008) 282.
[35] M.A. Meyers, A. Mistra and D.J. Benson // *Prog. Mater. Sci*. **51** (2006) 427.
[36] J. Schiřtz, F.D. Di Tolla and K.W. Jacobsen // *Nature* **39** (1998) 561.
[37] J. Schiřtz, T. Vegge, F.D. Di Tolla and K.W. Jacobsen // *Phys. Rev*. **B 60** (1999) 11971.
[38] H. V Swygenhoven and A. Caro // *Appl. Phys. Lett.* **71** (1997) 1652.
[39] H.V. Swygenhoven and A. Caro // *Phys. Rev. B* **58** (1998) 11246.
[40] H.V. Swygenhoven, A. Caro and. Farkas // *Mater. Sci. Engng.* **A309-310** (2001) 440.
[41] Y. Yamakov, D. Wolf, S.R. Phillpot and H. Gleiter // *Acta Mater.* **50** (2002) 61.
[42] J. Schiotz and K.W. Jacobsen // S*cience*. **301** (2003) 1357.
[43] J. Schiotz // S*cripta Mater.* **51** (2004) 837.
[44] A.C. Lund and C.A. Schuh // *Acta Mater*. **53** (2005) 3193.
[45] C. Zheng and Y.W. Zhang // *Mater. Sci. Engng.* **A 423** (2006) 97.
[46] G.A. Evangelakis, D.G. Papageorgiou, Ch.E. Lekka and I.E. Lagaris // *J. Alloys and Compounds* **434-435** (2007) 546.
[47] Z. Pan, Y. Li and Q. Wei // *Acta Mater.* (2008), doi:10.1016/i.actamat.2008.03.025.
[48] J.E. Carsley, J. Ning, W.M. Milligan, S.A. Hackney and E.C. Aifantis // *Nanostruct. Mater.* **5** (1995) 441.
[49] H.S. Kim, Y. Estrin and M.B. Bush // *Acta Mater*. **48** (2000) 493.
[50] M.A. Meyers, D.J. Benson and H.H. Fu, In: *Advanced Materials for the 21st Century*, ed. by Y-W. Chung, D.C. Dunand, P.K. Liaw and G.B. Olson (3M Soc., 1999), p. 499.
[51] D.J. Benson, H.H. Fu and M.A. Meyers // *Mater. Sci. Engng*. **A319-321** (2001) 854.
[52] H. Fu, D.J. Benson and M.A. Meyers // *Acta Mater*. **49** (2001) 2567.
[53] M.A. Meyers and E. Ashworth // *Phil. Mag*. **46** (1982) 737.
[54] B. Jiang and G.J. Weng // *Metall. Mater. Trans*. **34A** (2003) 765.
[55] B. Jiang and G.J. Weng // *Int. J. Plasticity* **20** (2004) 2007.
[56] B. Jiang and G.J. Weng // *J. Mech. Phys. Solids* **52** (2004) 1125.
[57] J. Li and G.J. Weng // *Int. J. Plasticity* **23** (2007) 2115.
[58] P. Barai and G.J. Weng // *Acta Mech*. **195** (2008) 327.
[59] P. Barai and G.J. Weng // *Int. J. Plasticity* **24** (2008) 1380.
[60] L. Capolungo, M. Cherkaoui and J. Qu // *ASME J. Engng. Mater. Tech*. **127** (2005) 400.
[61] L. Capolungo, C. Joachim, M. Cherkaoui and J. Qu // *Int. J. Plasticity* **21** (2005) 67.
[62] L. Capolungo, M. Cherkaoui and J. Qu // *Int. J. Plasticity* **23** (2007) 561.
[63] L. Capolungo, D.E. Spearot, M. Cherkaoui, D.L. McDowell, J. Qu and K.I. Jacob // *J. Mech. Phys. Solids* **55** (2007) 2300.
[64] R. Schwaiger, B. Moser, M. Dao, N. Chollacoop and S. Suresh // *Acta Mater*. **51** (2003) 5159.
[65] G.J. Weng // *Int. J. Engng. Sci***. 22** (1984) 845.
[66] G.J. Weng // *Int. J. Engng. Sci*. **28** (1990) 1111.
[67] G.J. Weng // *Int. J. Engng. Sci*. **30** (1992) 83.
[68] R.M. Christensen and K.H. Lo // *J. Mech. Phys. Solids* **27** (1979) 315; **34** (1986) 639.
[69] Z. Hashin and S. Shtrikman // *J. Mech. Phys. Solids* **11** (1963) 127.
[70] L.J. Walpole // *J. Mech. Phys. Solids* **14** (1966) 151, 289; **17** (1969) 235.
[71] G.J. Weng // *J. Mech. Phys. Solids* **31** (1983) 193.
[72] D.C. Drucker // *Q. Appl. Math.* **7** (1950) 411.
[73] M. Berveiller and A. Zaoui // *J. Mech. Phys. Solids* **26** (1979) 325.
[74] R. Hill // *J. Mech. Phys. Solids* **13** (1965) 89.
[75] G.J. Weng // *J. Appl. Mech*. **49** (1982) 728.
[76] J.W. Hutchinson // *Proc. R. Soc. London* **A325** (1970) 101.
[77] D.R.S. Talbot and J.R. Willis // *IMA J. Appl. Math*. **35** (1985) 39.
[78] G.P. Tandon and G.J. Weng // *J. App. Mech*. **55** (1988) 126.

[79] G.J. Weng // *J. Mech. Phys. Solids* **38** (1990) 419.
[80] P. Ponte Castańeda // *J. Mech. Phys. Solids* **39** (1991) 45.
[81] J.R. Willis // *J. Mech. Phys. Solids* **39** (1991) 73.
[82] Y.P. Qiu and G.J. Weng // *J. Appl. Mech*. **59** (1992) 261.
[83] P. Suquet // *C.R. Acad. Des Sci*., Ser. IIb **320** (1995) 563.
[84] G.K. Hu // *Int. J. Plasticity* **12** (1996) 439.
[85] M.L. Accorsi and S. Nemat-Nasser // *Mech. Mater*. **5** (1986) 209.
[86] G.J. Dvorak // *Proc. Roy. Soc. London* **A 437** (1992) 311.
[87] R. Masson, M. Bornert, P. Suquet and A. Zaoui // *J. Mech. Phys. Solids* **48** (2000) 1203.
[88] I. Doghri and L. Tinel // *Int. J. Plasticity* **21** (2005) 1919.
[89] S. Berbenni, V. Javier and M. Berveiller // *Int. J. Plasticity* **23** (2007) 114.
[90] S. Nemat-Nasser and M. Hori, *Micromechanics: Overall Properties of Heterogeneous Materials, 2nd ed*. (1999, Elsevier, Amsterdam).
[91] M. Bobeth and G. Diener // *J. Mech. Phys. Solids* **34** (1986) 1.
[92] W. Kreher and W. Pompe, *Internal Stress in Heterogeneous Solids* (Akademie, Berlin, 1989).
[93] Z. Hashin // *J. Appl. Mech*. **32** (1965) 630.
[94] Y.M. Wang and G.J. Weng // *J. Appl. Mech*. **59** (1992) 510.
[95] J. Li and G.J. Weng // *ASME J. Engng. Mater. Tech*. **116** (1994) 495.
[96] J. Li and G.J. Weng // *J. Mech. Phys. Solids* **45** (1997) 1069.
[97] J. Li and G.J. Weng // *Acta Mech*. **125** (1997) 141.
[98] J. Li and G.J. Weng // *Int. J. Plasticity* **14** (1998) 193.
[99] P.G. Sanders, M. Rittner, E. Kiedaish, J.R. Weertman, H. Kung and Y.C. Lu // *Nanostructured Mater*. **9** (1997) 433.
[100] A.S. Khan, H. Zhang and L. Takacs // *Int. J. Plasticity* **16** (2000) 1459.
[101] A.S. Khan and H. Zhang // *Int. J. Plasticity* **16** (2000) 1477.
[102] W.A. Spitzig, R.E. Smelser and O. Richmond // *Acta Metall*. **36** (1988) 1201.